

Bistatic Target Detection by Exploiting Both Deterministic Pilots and Unknown Random Data Payloads

Lei Xie, *Member, IEEE*, Fan Liu, *Senior Member, IEEE*, Shenghui Song, *Senior Member, IEEE*,
and Shi Jin, *Fellow, IEEE*

Abstract—Integrated sensing and communication (ISAC) plays a crucial role in 6G, to enable innovative applications such as drone surveillance, urban air mobility, and low-altitude logistics. However, the hybrid ISAC signal, which comprises *deterministic* pilot and *random* data payload components, poses challenges for target detection due to two reasons: 1) these two components cause coupled shifts in both the mean and variance of the received signal, and 2) the random data payloads are typically unknown to the sensing receiver in the bistatic setting. Unfortunately, these challenges could not be tackled by existing target detection algorithms. In this paper, a generalized likelihood ratio test (GLRT)-based detector is derived, by leveraging the known deterministic pilots and the statistical characteristics of the unknown random data payloads. Due to the analytical intractability of exact performance characterization, we perform an asymptotic analysis for the false alarm probability and detection probability of the proposed detector. The results highlight a critical trade-off: both deterministic and random components improve detection reliability, but the latter also brings statistical uncertainty that hinders detection performance. Simulations validate the theoretical findings and demonstrate the effectiveness of the proposed detector, which highlights the necessity of designing a dedicated detector to fully exploited the signaling resources assigned to random data payloads.

Index Terms—Integrated sensing and communications, Target detection, Random signals, False alarm probability, Detection Probability.

I. INTRODUCTION

The ongoing evolution of wireless communication networks toward the six generation (6G) is anticipated to provide essential support for many innovative applications such as drone surveillance, urban air mobility, and low-altitude logistics [1]–[3]. Among the core technological enablers of 6G, Integrated Sensing and Communication (ISAC) has emerged as a transformative paradigm that unifies radar sensing and wireless communication on the same platform [4]–[6]. ISAC facilitates the joint design and optimization of waveforms to serve both sensing and communication functions, maximizing spectral and hardware efficiency. Unlike traditional radar systems that transmit fully deterministic waveforms optimized solely for sensing, in current 5G New Radio (NR) standards, ISAC signals consist of both deterministic components (e.g., pilots) and random components (e.g. data payloads). Notably, pilots occupy only 0.15%–25% of system time-frequency resources, leaving the majority unused for sensing [7]. This motivates us

to enhance ISAC performance by leveraging the data payload for sensing purposes. However, the randomness introduced by data payloads adds uncertainty to the received signal, potentially degrading detection performance if not properly handled.

Target detection is an important topic for radar signal processing, particularly under challenging environmental conditions [8]–[12]. The classical formulation of this problem follows a binary hypothesis testing framework, in which the receiver distinguishes between the null hypothesis \mathcal{H}_0 (target absent) and the alternative hypothesis \mathcal{H}_1 (target present). Two principal statistical models have been widely adopted for this problem, i.e., the *first-order* and *second-order* models. In the first-order model, the target signature is assumed to be deterministic [13]–[16], and its presence induces a mean shift in the received signal. In contrast, the second-order model treats the target signature as a random process [17]–[20], leading to a change in the covariance of received signal while the mean remains unchanged. Beyond these classical models, recent work introduced a *hybrid model* [21], where the target signature contains both a deterministic component and a statistically independent random perturbation. In this setting, the deterministic component affects the signal mean, while the perturbation influences the covariance structure, offering a more flexible and realistic representation.

While the classical models provide foundation for developing detection strategies, their direct application to ISAC systems is nontrivial. In particular, the randomness inherent in ISAC signals introduces two key challenges for target detection: 1) **Hybrid signal model**: Both the deterministic pilots and random data payloads are reflected by the target. The deterministic component induces a shift in the mean of the received signal, while the random component contributes to its variance. This results in a detection problem that fits within the hybrid model framework. However, unlike conventional hybrid models where the shifts in mean and covariance are typically assumed to be statistically independent [21], both are coupled in ISAC systems due to their dependence on the unknown path gain. This complicates the statistical characterization of the received signal and poses significant challenges for deriving detectors. 2) **Unknown data payloads at the sensing receiver**: Collaborative sensing has become a key focus in many networked ISAC systems due to its ability to extend coverage and improve detection performance [6]. However, the sensing receiver is spatially separated from the transmitter in collaborative sensing. In such cases, the transmitted data payloads are unknown to the sensing receiver [22], complicating coherent detection and parameter estimation from reflected

L. Xie is with School of Cyber Science and Engineering, Southeast University, Nanjing, China. F. Liu and S. Jin are with the National Mobile Communications Research Laboratory, Southeast University, Nanjing, China. S. Song is with the Division of Integrative Systems and Design and the Department of Electronic and Computer Engineering, the Hong Kong University of Science and Technology.

signals. One possible solution is to forward the transmitted signal to the sensing receiver via a dedicated backhaul link [23], [24], but this introduces substantial communication overhead and raises concerns related to latency, privacy, and security. 3) **Lack of detection-based metrics**: Although ISAC systems have attracted growing research attention, most existing works focused on estimation-based metrics such as the Bayesian Cramér-Rao Bound (CRB) [25], ergodic linear minimum mean-square error (ELMMSE) [26], sensing mutual information (SMI) [27], and the expectation of the integrated sidelobe level (EISL) [28]. While these metrics provide valuable insights into average estimation performance, they are generally unable to characterize the fundamental performance of target detection.

In this paper, we focus on two critical and open research questions: 1) How can we design an effective detector with partial knowledge of the ISAC signal? and 2) What is the achievable target detection performance of the proposed detector? To answer these research questions, we consider a bistatic ISAC system where the transmitter emits a superimposed signal consisting of a deterministic component and a random component. Within each frame, the sensing receiver is assumed to have perfect knowledge of the deterministic component but only statistical information of the random component. We first derive a generalized likelihood ratio test (GLRT) detector tailored to this specific hybrid signal model. Then, we analyze the detection performance in terms of false alarm probability (FAP) and detection probability (DP). Given the analytical intractability of the exact performance evaluation, we perform an asymptotic analysis in the large-sample regime. Simulation results demonstrate the effectiveness of the proposed detector and confirm the accuracy of the asymptotic approximations, even in moderate regimes.

The main contributions of this paper are summarized as:

- 1) We propose a new hypothesis testing tailored for the hybrid signal model with mixed deterministic-random components. Then, we derive the corresponding GLRT-based detector, which leverages the known deterministic component and the statistical information of the random component.
- 2) Due to the difficulty to achieve exact performance analysis with finite samples, we conduct a performance analysis in the asymptotic regime, where the number of samples tends to infinity. The asymptotic results regarding FAP and DP are shown to be accurate even in moderate-sample regimes.
- 3) The performance analysis reveals a key trade-off in the hybrid signal: both deterministic and random components improve detection reliability, but the latter also brings statistical uncertainty that hinders detection performance.

The remainder of the paper is organized as follows. Section II presents the system model. Section III derives the GLRT-based detector with random ISAC signals. Section IV studies the false alarm and detection probability in the asymptotic region and provides some physical insights. Simulation results are given in Section V to validate the effectiveness of the

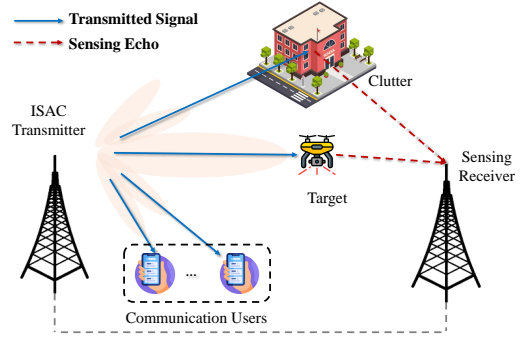


Fig. 1. Illustration of the considered ISAC system.

proposed detector and the accuracy of the theoretical results. Finally, Section VII concludes the paper, summarizing the key findings.

II. SYSTEM MODEL

In this paper, we investigate the problem of simultaneous downlink communication and target detection based on a bistatic sensing architecture, as illustrated in Fig. 1. Specifically, we consider an ISAC system comprising an ISAC transmitter equipped with N antennas, K single-antenna communication users, and a separate sensing receiver equipped with M antennas. The ISAC transmitter emits a unified waveform that serves the dual purpose of delivering data payloads to users and sensing the environment. At the receiver side, each communication user aims to decode its intended message, while the sensing receiver is responsible for detecting the presence of target of interest (TOI) in a cluttered environment. In the following, we detail the models for both the transmitted and received signals.

A. Transmitted signal

As shown in Fig. 2, each frame consists of L samples, partitioned into L_p deterministic pilots and L_d random data symbols. Without loss of generality, we assume $L_p > N$ and $L_d > N$. In the considered ISAC framework, communication is enabled through random data symbols, while target detection leverages the deterministic pilots and the random data payload. In practice, the transmit signals are typically interleaved according to predefined strategies or protocols, such as quasi-periodic placement (QPP) schemes [29]. In particular, the transmitted signal is given by [30]

$$\mathbf{X} \triangleq [\mathbf{X}_p, \mathbf{X}_d] \mathbf{J} = \mathbf{X}_p \mathbf{J}_p + \mathbf{X}_d \mathbf{J}_d, \quad (1)$$

where $\mathbf{J} = [\mathbf{J}_p^T, \mathbf{J}_d^T]^T \in \mathbb{C}^{L \times L}$ is a permutation matrix which depends on the frame structure, $\mathbf{J}_p \in \mathbb{C}^{L_p \times L}$ and $\mathbf{J}_d \in \mathbb{C}^{L_d \times L}$ denotes the first L_p and the last L_d rows of \mathbf{J} , respectively. Since \mathbf{J} is an orthogonal matrix, it follows that $\mathbf{J}_p \mathbf{J}_p^T = \mathbf{I}$ and $\mathbf{J}_d \mathbf{J}_d^T = \mathbf{I}$.

The pilot component is defined by

$$\mathbf{X}_p = \mathbf{F}_p \mathbf{S}_p \in \mathbb{C}^{N \times L_p}, \quad (2)$$

where $\mathbf{F}_p \in \mathbb{C}^{N \times 1}$ is the sensing precoding vector, and \mathbf{S}_p denotes the pilot symbols. In the considered system, all

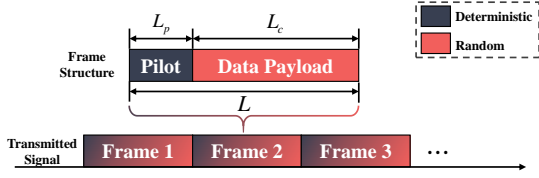


Fig. 2. Illustration of the frame structure.

pilot signals are transmitted toward the direction of the TOI. During this period, the system operates as a phased array. Accordingly, we define the precoding matrix as $\mathbf{F}_p = \mathbf{f}_p \mathbf{1}_N^T$, where \mathbf{f}_p denotes the beamformer towards TOI. This leads to the transmit signal matrix:

$$\mathbf{X}_p = (\mathbf{f}_p \mathbf{1}_N^T) \mathbf{S}_p = \mathbf{f}_p \mathbf{S}_p^T, \quad (3)$$

where $\mathbf{s}_p = \mathbf{S}_p^T \mathbf{1}_N$ represents the aggregated pilot symbols. Without loss of generality, each pilot symbol is assumed to have unit module, i.e., $|s_{s,l}| = 1$ [31]. We assume that $\|\mathbf{f}_p\|^2 = \frac{P_p}{L_p}$, such that $\|\mathbf{X}_p\|^2 = P_p < \infty$. Note that \mathbf{X}_p is deterministic and thus known to the sensing receiver.

The data payload is given by

$$\mathbf{X}_d = \mathbf{F}_d \mathbf{S}_d \in \mathbb{C}^{N \times L_d}, \quad (4)$$

where $\mathbf{F}_d \in \mathbb{C}^{N \times N}$ is the communication precoding vector with $\|\mathbf{F}_d\|_F^2 = \frac{P_d}{L_d}$, and $\mathbf{S}_d \in \mathbb{C}^{N \times L_d}$ represents the data symbol matrix whose entries are independently and identically distributed (i.i.d.) with zero mean and unit variance, i.e., $[\mathbf{S}_d]_{i,j} \sim \mathcal{CN}(0, 1)$. In this paper, the communication symbols are assumed to be unknown to the sensing receiver.

B. Received signal

The clutter channel without the target is modeled as

$$\mathbf{H}_e = \sum_{n=1}^{N_{\text{path}}} \varepsilon_n \mathbf{a}_n \mathbf{b}_n^H, \quad (5)$$

where N_{path} denotes the number of paths in the environment, ε_n , \mathbf{a}_n , and \mathbf{b}_n represent the path loss, the transmit steering vector, and the receive steering vector of the n th path, respectively¹. The received signal at the sensing receiver under two hypotheses is thus given by

$$\begin{aligned} \mathcal{H}_0 : \mathbf{Y} &= \underbrace{\mathbf{H}_e \mathbf{X}}_{\text{Environment}} + \mathbf{N} \in \mathbb{C}^{M \times 1}, \\ \mathcal{H}_1 : \mathbf{Y} &= \underbrace{\alpha \mathbf{a}_t \mathbf{b}_t^H \mathbf{X}}_{\text{Target}} + \underbrace{\mathbf{H}_e \mathbf{X}}_{\text{Environment}} + \mathbf{N} \in \mathbb{C}^{M \times 1}, \end{aligned} \quad (6)$$

where α , \mathbf{a}_t and \mathbf{b}_t denote the path gain, the transmit and receive steering vectors of the TOI, respectively, and \mathbf{N} represents the additive white Gaussian noise (AWGN), whose entries are i.i.d. with zero mean and variance σ^2 , i.e.,

¹In this paper, we assume that the clutter channel remains unchanged throughout the frame. This quasi-static channel assumption is commonly adopted in ISAC literature [32], [33].

$[\mathbf{N}]_{i,j} \sim \mathcal{CN}(0, \sigma^2)$. By substituting (1) into (6), the resulting received signal can be reformulated by

$$\begin{aligned} \mathcal{H}_0 : \mathbf{Y} &= \underbrace{\mathbf{H}_e \mathbf{f}_p \mathbf{s}_p^T \mathbf{J}_p}_{\text{Deterministic}} + \underbrace{\mathbf{H}_e \mathbf{F}_d \mathbf{S}_d^T}_{\text{Random}} + \mathbf{N}, \\ \mathcal{H}_1 : \mathbf{Y} &= \underbrace{\alpha (\mathbf{b}_t^H \mathbf{f}_p) \mathbf{a}_t \mathbf{s}_p^T \mathbf{J}_p}_{\text{Deterministic}} + \underbrace{\mathbf{H}_e \mathbf{f}_p \mathbf{s}_p^T \mathbf{J}_p}_{\text{Random}} \\ &\quad + \underbrace{\alpha \mathbf{a}_t \mathbf{b}_t^H \mathbf{F}_d \mathbf{S}_d^T + \mathbf{H}_e \mathbf{F}_d \mathbf{S}_d^T}_{\text{Random}} + \mathbf{N}. \end{aligned} \quad (7)$$

III. GLRT WITH HYBRID SIGNALS

In this section, we derive the proposed detector based on the GLRT framework. The detector is designed to address the hybrid nature of integrated sensing and communication (ISAC) signals, i.e., consisting of both deterministic and random components that propagate through the same channel. As a result, the presence of a target will lead to simultaneous shifts in both the mean and covariance structure of the received signal.

Based on the received signal model in (7), we consider the following binary hypothesis testing framework:

$$\begin{aligned} \mathcal{H}_0 : \mathbf{Y} &\sim \mathcal{CN}(\mathbf{U}, \mathbf{\Sigma}), \\ \mathcal{H}_1 : \mathbf{Y} &\sim \mathcal{CN}(\mathbf{U} + \Delta \mathbf{U}(\alpha), \mathbf{\Sigma} + \Delta \mathbf{\Sigma}(\alpha)), \end{aligned} \quad (8)$$

where the mean and covariance under the null hypothesis \mathcal{H}_0 are given by

$$\mathbf{U} \triangleq \mathbf{H}_e \mathbf{f}_p \mathbf{s}_p^T \mathbf{J}_p, \quad \mathbf{\Sigma} \triangleq L_d \mathbf{H}_e \mathbf{F}_d \mathbf{F}_d^H \mathbf{H}_e^H + L \sigma^2 \mathbf{I}. \quad (9)$$

Under the alternative hypothesis \mathcal{H}_1 , two additional terms appear in the mean and covariance of the received signal, respectively:

$$\Delta \mathbf{U}(\alpha) \triangleq \alpha \lambda_p \mathbf{a}_t \mathbf{s}_p^T \mathbf{J}_p, \quad \Delta \mathbf{\Sigma}(\alpha) \triangleq L_d |\alpha|^2 |\lambda_d|^2 \mathbf{a}_t \mathbf{a}_t^H, \quad (10)$$

where

$$\lambda_p = \mathbf{b}_t^H \mathbf{f}_p, \quad |\lambda_d|^2 = \mathbf{b}_t^H \mathbf{F}_d \mathbf{F}_d^H \mathbf{b}_t. \quad (11)$$

In particular, the additional mean $\Delta \mathbf{U}(\alpha)$ originates from the echo of the deterministic pilots, while the additional covariance $\Delta \mathbf{\Sigma}(\alpha)$ arises from the random data payloads. It can be observed that the deterministic and random components contribute to different statistical characteristics of the received signals. Consequently, under \mathcal{H}_1 , both the mean and variance of the observed signal are different from those under \mathcal{H}_0 . Furthermore, in contrast to traditional detection models where the two additional components are assumed to be independent [21], they are correlated through an unknown coefficient α . This dependence poses challenges for the design and analysis of optimal detectors.

Before further proceeding, we introduce two normalized intermediate quantities:

$$\bar{\mathbf{f}}_p = L_p^{\frac{1}{2}} \mathbf{f}_p, \quad \bar{\mathbf{F}}_d = L_d^{\frac{1}{2}} \mathbf{F}_d, \quad (12)$$

such that $\|\bar{\mathbf{f}}_p\|^2 = L_p \|\mathbf{f}_p\|^2 = P_p < \infty$, and $\|\bar{\mathbf{F}}_d\|^2 = L_d \|\mathbf{F}_d\|^2 = P_d < \infty$. Then, we have

$$|\bar{\lambda}_p|^2 \triangleq |\mathbf{b}_t^H \bar{\mathbf{f}}_p|^2 \stackrel{(a)}{\leq} P_p \|\mathbf{b}_t\|^2 < \infty, \quad (13)$$

$$|\bar{\lambda}_d|^2 \triangleq \mathbf{b}_t^H \bar{\mathbf{F}}_d \bar{\mathbf{F}}_d^H \mathbf{b}_t \stackrel{(b)}{\leq} P_d \|\mathbf{b}_t\|^2 < \infty, \quad (14)$$

where (a) and (b) follow from the Cauchy–Schwarz inequality. Meanwhile, it can be obtained that $|\bar{\lambda}_p|^2 = L_p |\lambda_p|^2$ and $|\bar{\lambda}_d|^2 = L_d |\lambda_d|^2$. Moreover, we assume that $\frac{|\bar{\lambda}_d|}{|\bar{\lambda}_p|} \in (0, \infty)$ to avoid the pilot-only or data payload-only cases.

In the following, we derive the corresponding GLRT-based detector, which is a widely used detection framework in radar signal processing, particularly with partially-unknown signal parameters [10], [14]. By performing maximum likelihood (ML) estimation of α , GLRT constructs a test statistic based on the ratio of the likelihoods under \mathcal{H}_1 and \mathcal{H}_0 :

$$\Lambda = \frac{\max_{\alpha} f_{\mathbf{Y}|\mathcal{H}_1}(\mathbf{Y}; \alpha | \mathcal{H}_1)}{f_0(\mathbf{Y})} \underset{\mathcal{H}_0}{\underset{\mathcal{H}_1}{\geq}} \eta, \quad (15)$$

where

$$f_{\mathbf{Y}|\mathcal{H}_1}(\mathbf{Y}; \alpha | \mathcal{H}_1) = \frac{e^{-\text{tr}[(\boldsymbol{\Sigma} + \Delta \boldsymbol{\Sigma}(\alpha))^{-1}(\mathbf{Y} - \mathbf{U} - \Delta \mathbf{U}(\alpha))(\mathbf{Y} - \mathbf{U} - \Delta \mathbf{U}(\alpha))^H]}}{\pi^N \det(\boldsymbol{\Sigma} + \Delta \boldsymbol{\Sigma}(\alpha))}, \quad (16)$$

$$f_{\mathbf{Y}|\mathcal{H}_0}(\mathbf{Y} | \mathcal{H}_0) = \frac{e^{-\text{tr}[\boldsymbol{\Sigma}^{-1}(\mathbf{Y} - \mathbf{U})(\mathbf{Y} - \mathbf{U})^H]}}{\pi^N \det(\boldsymbol{\Sigma})}, \quad (17)$$

denote the probability density functions (PDFs) of \mathbf{Y} under \mathcal{H}_1 and \mathcal{H}_0 , respectively, and η is a given detection threshold. By taking the logarithm of Λ , we have²

$$\log \Lambda = \frac{|\alpha|^2 |\bar{\lambda}_d|^2 \|\boldsymbol{\mu}\|^2}{1 + |\alpha|^2 |\bar{\lambda}_d|^2 \beta} + \frac{2\Re(\alpha \gamma^*)}{1 + |\alpha|^2 |\bar{\lambda}_d|^2 \beta} - \frac{|\alpha|^2 |\bar{\lambda}_p|^2 \beta}{1 + |\alpha|^2 |\bar{\lambda}_d|^2 \beta} - \log(1 + |\alpha|^2 |\bar{\lambda}_d|^2 \beta), \quad (18)$$

where

$$\beta = \mathbf{a}_t^H \boldsymbol{\Sigma}^{-1} \mathbf{a}_t, \quad (19a)$$

$$\boldsymbol{\mu} = (\mathbf{Y} - \mathbf{U})^H \boldsymbol{\Sigma}^{-1} \mathbf{a}_t, \quad (19b)$$

$$\gamma = \lambda_p^* \boldsymbol{\mu}^H \mathbf{J}_p^T \mathbf{s}_p^* = \lambda_p^* \mathbf{a}_t^H \boldsymbol{\Sigma}^{-1} (\mathbf{Y} - \mathbf{U}) \mathbf{J}_p^T \mathbf{s}_p^*. \quad (19c)$$

Since the complex amplitude α is an unknown parameter, the first step in deriving the GLRT framework is to identify the value of α that maximizes the likelihood function $f_{\mathbf{Y}|\mathcal{H}_1}(\mathbf{Y}; \alpha | \mathcal{H}_1)$. Accordingly, we introduce the following proposition to characterize the maximizer of the likelihood function with respect to α , denoted by

$$\alpha_{\dagger} \triangleq \arg \max_{\alpha} f_{\mathbf{Y}|\mathcal{H}_1}(\mathbf{Y}; \alpha | \mathcal{H}_1). \quad (20)$$

Lemma 1: The maximizer α_{\dagger} is given by

$$\alpha_{\dagger} = Q_{\dagger} \gamma, \quad (21)$$

where

$$Q_{\dagger} = -\frac{1}{3|\bar{\lambda}_d|^2 \beta} + \sqrt[3]{\Delta_1 + \sqrt{\Delta_1^2 + \Delta_2^3}} + \sqrt[3]{\Delta_1 - \sqrt{\Delta_1^2 + \Delta_2^3}}, \quad (22)$$

²In this paper, the clutter-plus-noise covariance matrix $\boldsymbol{\Sigma}$ is known a priori through prior estimation.

with

$$\Delta_1 = -\frac{(|\bar{\lambda}_p|^2 + |\bar{\lambda}_d|^2) \beta - \|\boldsymbol{\mu}\|^2 |\bar{\lambda}_d|^2}{6|\bar{\lambda}_d|^6 |\gamma|^2 \beta^3} - \frac{1}{27|\bar{\lambda}_d|^6 \beta^3} - \frac{1}{2|\bar{\lambda}_d|^4 |\gamma|^2 \beta}, \quad (23)$$

$$\Delta_2 = \frac{(|\bar{\lambda}_p|^2 + |\bar{\lambda}_d|^2) \beta - \|\boldsymbol{\mu}\|^2 |\bar{\lambda}_d|^2}{3|\bar{\lambda}_d|^4 |\gamma|^2 \beta^2} - \frac{1}{9|\bar{\lambda}_d|^4 \beta^2}. \quad (24)$$

Proof: See Appendix A. \blacksquare

By invoking **Lemma 1**, the corresponding GLRT is given by

$$\tau(\mathbf{Y}) \triangleq \log \Lambda \underset{\mathcal{H}_0}{\underset{\mathcal{H}_1}{\geq}} \log \eta, \quad (25)$$

where

$$\tau(\mathbf{Y}) = \frac{Q_{\dagger}^2 |\bar{\lambda}_d|^2 |\gamma|^2 \|\boldsymbol{\mu}\|^2}{1 + Q_{\dagger}^2 |\bar{\lambda}_d|^2 |\gamma|^2 \beta} + \frac{2Q_{\dagger} |\gamma|^2}{1 + Q_{\dagger}^2 |\bar{\lambda}_d|^2 |\gamma|^2 \beta} - \frac{LQ_{\dagger}^2 |\lambda_p|^2 |\gamma|^2 \beta}{1 + Q_{\dagger}^2 |\bar{\lambda}_d|^2 |\gamma|^2 \beta} - \log(1 + Q_{\dagger}^2 |\bar{\lambda}_d|^2 |\gamma|^2 \beta). \quad (26)$$

Remark 1 (Pilot-only detector): By setting $L_d = 0$, $L_p = L$, and $\mathbf{F}_d = \mathbf{0}$, the ISAC system reduces to a conventional radar system that transmits only deterministic sensing signals. In such a pilot-only case, the corresponding detector can be derived from (26):

$$\tau_0(\mathbf{Y}) = \frac{|\mathbf{a}_t^H \boldsymbol{\Sigma}_p^{-1} (\mathbf{Y} - \mathbf{U}) \mathbf{J}_p^T \mathbf{s}_p^*|^2}{L |\mathbf{a}_t^H \boldsymbol{\Sigma}_p^{-1} \mathbf{a}_t|}, \quad (27)$$

where $\boldsymbol{\Sigma}_p = \boldsymbol{\Sigma}|_{L_d=0} = L\sigma^2 \mathbf{I}$. As will be shown in the simulations, neglecting the random component and directly applying the pilot-only detector in (27) leads to significantly degraded detection performance.

Remark 2 (Data Payload-only detector): By setting $L_p = 0$, $L_d = L$, and $\mathbf{F}_p = \mathbf{0}$, the data payload-only detector is

$$\tau_0(\mathbf{Y}) = \frac{\|\mathbf{Y}^H \boldsymbol{\Sigma}_d^{-1} \mathbf{a}_t\|^2}{|\mathbf{a}_t^H \boldsymbol{\Sigma}_d^{-1} \mathbf{a}_t|} - 1 - \log\left(\frac{\|\mathbf{Y}^H \boldsymbol{\Sigma}_d^{-1} \mathbf{a}_t\|^2}{|\mathbf{a}_t^H \boldsymbol{\Sigma}_d^{-1} \mathbf{a}_t|}\right), \quad (28)$$

where $\boldsymbol{\Sigma}_d = L\mathbf{H}_e \mathbf{F}_d \mathbf{F}_d^H \mathbf{H}_e^H + L\sigma^2 \mathbf{I}$.

IV. PERFORMANCE ANALYSIS

In this section, we provide performance analysis of the proposed detector. Due to the analytical intractability of exact performance characterization with finite samples, we focus on the asymptotic regime where L tends to infinity. It will be demonstrated later that the results remain accurate even for small values of L . This analysis offers insight into the asymptotic behavior of the proposed detector and serves to reveal the impact of key system parameters.

A. False Alarm Probability

Under \mathcal{H}_0 , the received signal \mathbf{Y} can be rewritten by

$$\mathbf{Y} = \mathbf{U} + \bar{\boldsymbol{\Sigma}}^{\frac{1}{2}} \mathbf{Z}, \quad (29)$$

where $\bar{\boldsymbol{\Sigma}} \triangleq \frac{1}{L} \boldsymbol{\Sigma} = \frac{L_d}{L} \mathbf{H}_e \mathbf{F}_d \mathbf{F}_d^H \mathbf{H}_e^H + \sigma^2 \mathbf{I}$, and \mathbf{Z} is random with i.i.d. Gaussian entries of mean 0 and variance 1.

The analysis of the false alarm probability relies on characterizing the asymptotic behavior of the test statistic $\tau(\mathbf{Y})$, due to the randomness of the received signal \mathbf{Y} . To this end, we begin by investigating the asymptotic properties of the quantities $\boldsymbol{\mu}$ and γ , both of which are dependent on \mathbf{Y} , as established in the following two lemmas.

Lemma 2: The mean and variance of $\frac{\|\boldsymbol{\mu}\|^2}{\beta}$ are respectively given by

$$\mathbb{E}\left(\frac{\|\boldsymbol{\mu}\|^2}{\beta}\right) = L^{-1}\mathbb{E}\left(\frac{\|\bar{\boldsymbol{\mu}}\|^2}{\bar{\beta}}\right) = 1, \quad (30)$$

$$\text{var}\left(\frac{\|\boldsymbol{\mu}\|^2}{\beta}\right) = L^{-2}\text{var}\left(\frac{\|\bar{\boldsymbol{\mu}}\|^2}{\bar{\beta}}\right) = L^{-1}, \quad (31)$$

where

$$\bar{\beta} = \mathbf{a}_t^H \bar{\boldsymbol{\Sigma}}^{-1} \mathbf{a}_t, \quad (32a)$$

$$\bar{\boldsymbol{\mu}} = (\mathbf{Y} - \mathbf{U})^H \bar{\boldsymbol{\Sigma}}^{-1} \mathbf{a}_t. \quad (32b)$$

For all $\delta > 0$, we have

$$\sup_{\mathbf{Y}} L^{\frac{1}{2}-\delta} \left| \frac{\|\boldsymbol{\mu}\|^2}{\beta} - 1 \right| \xrightarrow[L \rightarrow \infty]{a.s.} 0. \quad (33)$$

Proof: See Appendix B.

Lemma 2 reflects the energy of the received signal projected onto the known target direction, normalized by a scale factor that accounts for noise and interference. On average, the quantity $\frac{\|\boldsymbol{\mu}\|^2}{\beta}$ converges to 1, indicating it is an unbiased measure under the concerned signal model. Furthermore, its variability decreases with L , which implies that with more signal samples, $\frac{\|\boldsymbol{\mu}\|^2}{\beta}$ becomes concentrated on its expectation.

Lemma 3: The mean and variance of $|\gamma|^2$ are respectively given by

$$\mu_\Gamma \triangleq \mathbb{E}(\Gamma) = L^{-2}|\bar{\lambda}_p|^2\bar{\beta}, \quad (34)$$

$$\sigma_\Gamma^2 \triangleq \text{var}(\Gamma) = L^{-4}|\bar{\lambda}_p|^4\bar{\beta}^2, \quad (35)$$

where

$$\bar{\gamma} = \lambda_p^* \bar{\boldsymbol{\mu}}^H \mathbf{J}_p^T \mathbf{s}_p^*. \quad (36)$$

For all integer $p > 0$ and $\delta > 0$, we have

$$\sup_{\mathbf{Y}} L^{2p-\delta} \left| |\gamma|^2 - L^{-2}|\bar{\lambda}_p|^2\bar{\beta} \right|^p \xrightarrow[L \rightarrow \infty]{a.s.} 0. \quad (37)$$

Proof: See Appendix C.

It is worth noting that the expression of Q_\dagger is highly complex, thereby rendering the performance analysis analytically challenging. To facilitate the analysis, we introduce an approximation of Q_\dagger in the following proposition:

Proposition 1: Under \mathcal{H}_0 , as $L \rightarrow \infty$, we have

$$Q_\dagger \xrightarrow[L \rightarrow \infty]{a.s.} \tilde{Q}_\dagger \triangleq \frac{1}{L^{-1}|\bar{\lambda}_p|^2\bar{\beta}} \quad (38)$$

Proof: See Appendix D.

With these notations at hand, we are now ready to analyze the asymptotic behavior of the GLRT under \mathcal{H}_0 hypothesis in the following proposition.

Proposition 2: As $L \rightarrow \infty$, we have

$$\tau(\mathbf{Y}|\mathcal{H}_0) \xrightarrow[L \rightarrow \infty]{a.s.} \tilde{\tau}(\mathbf{Y}|\mathcal{H}_0) \triangleq \varrho_0|\gamma|^2 + \zeta_0, \quad (39)$$

where

$$\varrho_0 = \frac{L}{|\bar{\lambda}_p|^2\bar{\beta}}, \quad \zeta_0 = \frac{|\bar{\lambda}_d|^2}{L|\bar{\lambda}_p|^2} - \log\left(1 + \frac{|\bar{\lambda}_d|^2}{L|\bar{\lambda}_p|^2}\right). \quad (40)$$

Proof: See Appendix E.

Notably, the relationship between $\tau(\mathbf{Y}|\mathcal{H}_0)$ and $|\gamma|^2$ is non-linear, which hinders the derivation of the FAP. To this end, we approximate $\tau(\mathbf{Y}|\mathcal{H}_0)$ by employing its first-order Taylor's expansion $\tilde{\tau}(\mathbf{Y}|\mathcal{H}_0)$ in **Proposition 2**, by utilizing the fact that higher-order terms are significantly smaller than the first-order term in the asymptotic regime. The FAP of the proposed GLRT-based detector is shown in the following corollary.

Corollary 1: The false alarm probability is given by

$$\mathbb{P}_{\text{fa}} = e^{-L \log \eta + \frac{|\bar{\lambda}_d|^2}{|\bar{\lambda}_p|^2} - L \log\left(1 + \frac{|\bar{\lambda}_d|^2}{L|\bar{\lambda}_p|^2}\right)}. \quad (41)$$

Proof: Since $|\gamma|^2$ follows the Gamma distribution with a shape parameter 1 and a scale parameter $L^{-2}|\bar{\lambda}_p|^2\bar{\beta}$, we have

$$\begin{aligned} \mathbb{P}_{\text{fa}} &= \mathbb{P}(\tau(\mathbf{Y}) > \log \eta | \mathcal{H}_0) \\ &= \mathbb{P}\left(|\gamma|^2 > \frac{\log \eta - \zeta_0}{\varrho_0} \middle| \mathcal{H}_0\right) = e^{-\frac{\log \eta - \zeta_0}{\varrho_0(L^{-2}|\bar{\lambda}_p|^2\bar{\beta})}} \\ &= e^{-L \log \eta + \frac{|\bar{\lambda}_d|^2}{|\bar{\lambda}_p|^2} - L \log\left(1 + \frac{|\bar{\lambda}_d|^2}{L|\bar{\lambda}_p|^2}\right)}, \end{aligned} \quad (42)$$

which completes the proof. \blacksquare

Remark 3 (Performance Degradation): The FAP of the conventional radar system defined in (27) is given by

$$\tilde{\mathbb{P}}_{\text{fa}} = e^{-L \log \eta}. \quad (43)$$

Therefore, we have

$$\mathbb{P}_{\text{fa}} = e^{\frac{|\bar{\lambda}_d|^2}{|\bar{\lambda}_p|^2} - L \log\left(1 + \frac{|\bar{\lambda}_d|^2}{L|\bar{\lambda}_p|^2}\right)} \tilde{\mathbb{P}}_{\text{fa}}. \quad (44)$$

Moreover, since $\frac{|\bar{\lambda}_d|^2}{|\bar{\lambda}_p|^2} \geq 0$, it follows that $\mathbb{P}_{\text{fa}} \geq \tilde{\mathbb{P}}_{\text{fa}}$. This reveals two physical insights: 1) the conventional radar system achieves the lowest FAP, which can thus serve as a lower bound, and 2) to ensure a constant FAP, the detection threshold must be adaptively adjusted to mitigate the adverse effects of data payload-induced randomness on the sensing performance. This motivates us to derive the detection threshold in the following corollary.

Corollary 2: In order to satisfy a fixed false alarm probability \mathbb{P}_{fa} , the decision threshold η can be given by

$$\eta = e^{\frac{|\bar{\lambda}_d|^2}{L|\bar{\lambda}_p|^2} - \log\left(1 + \frac{|\bar{\lambda}_d|^2}{L|\bar{\lambda}_p|^2}\right) - \frac{\ln \mathbb{P}_{\text{fa}}}{L}}. \quad (45)$$

It can be observed from (45) that the target false alarm rate can be maintained by adjusting the number of samples L and the deterministic-to-random power ratio $\frac{|\bar{\lambda}_d|^2}{|\bar{\lambda}_p|^2}$.

B. Detection Probability

Under \mathcal{H}_1 , the received signal \mathbf{Y} can be given by

$$\mathbf{Y} = \mathbf{U} + \Delta \mathbf{U}(\alpha) + (\bar{\boldsymbol{\Sigma}} + \Delta \bar{\boldsymbol{\Sigma}}(\alpha))^{\frac{1}{2}} \mathbf{Z}, \quad (46)$$

where $\Delta \bar{\boldsymbol{\Sigma}}(\alpha) \triangleq L^{-1} \Delta \boldsymbol{\Sigma}(\alpha) = L^{-1}|\alpha|^2|\bar{\lambda}_d|^2\mathbf{a}_t\mathbf{a}_t^H$. To facilitate the evaluation of DP, we give the following lemmas regarding the mean and variance of $\frac{\|\boldsymbol{\mu}\|^2}{\beta}$.

Lemma 4: The mean and variance of $\frac{\|\boldsymbol{\mu}\|^2}{\beta}$ are respectively given by

$$\mathbb{E}\left(\frac{\|\boldsymbol{\mu}\|^2}{\beta}\right) = 1 + L^{-1}|\alpha|^2 (|\bar{\lambda}_p|^2 + |\bar{\lambda}_d|^2) \bar{\beta}, \quad (47)$$

$$\text{var}\left(\frac{\|\boldsymbol{\mu}\|^2}{\beta}\right) = L^{-1}(\kappa^2 + 2L^{-1}\kappa|\alpha|^2|\bar{\lambda}_p|^2\bar{\beta}), \quad (48)$$

where

$$\kappa = 1 + L^{-1}|\alpha|^2|\bar{\lambda}_d|^2\bar{\beta}. \quad (49)$$

For all $\delta > 0$, we have

$$\sup_{\mathbf{Y}} L^{\frac{1}{2}-\delta} \left| \frac{\|\boldsymbol{\mu}\|^2}{\beta} - \hat{\mu} \right| \xrightarrow[L \rightarrow \infty]{a.s.} 0. \quad (50)$$

where $\hat{\mu} = 1 + L^{-1}|\alpha|^2 (|\bar{\lambda}_p|^2 + |\bar{\lambda}_d|^2) \bar{\beta}$.

Proof: See Appendix F.

Lemma 5: The mean and variance of $|\gamma|^2$ are respectively given by

$$\mu_{\Gamma} = L^{-2}\kappa|\bar{\lambda}_p|^2\bar{\beta} + L^{-2}|\alpha|^2|\bar{\lambda}_p|^4\bar{\beta}^2, \quad (51)$$

$$\sigma_{\Gamma}^2 = L^{-4}\kappa^2|\bar{\lambda}_p|^4\bar{\beta}^2 + 2L^{-4}\kappa|\alpha|^2|\bar{\lambda}_p|^6\bar{\beta}^3. \quad (52)$$

For all integer $p > 0$ and $\delta > 0$, we have

$$\sup_{\mathbf{Y}} L^{\frac{p}{2}-\delta} \left| |\gamma|^2 - \mathbb{E}(|\gamma|^2) \right|^p \xrightarrow[L \rightarrow \infty]{a.s.} 0, \quad (53)$$

Proof: See Appendix G.

With **Lemmas 4 & 5**, we can obtain the asymptotic behavior of the GLRT under the \mathcal{H}_1 hypothesis, as presented in the following proposition.

Proposition 3: As $L \rightarrow \infty$, we have

$$\tau(\mathbf{Y}|\mathcal{H}_1) \xrightarrow[L \rightarrow \infty]{a.s.} \tilde{\tau}(\mathbf{Y}|\mathcal{H}_1) \triangleq \varrho_1|\gamma|^2 + \zeta_1, \quad (54)$$

where

$$\varrho_1 = \frac{L}{|\bar{\lambda}_p|^2\bar{\beta}}, \quad (55)$$

$$\zeta_1 = \frac{(1 + |\alpha|^2|\bar{\lambda}_p|^2\bar{\beta})|\bar{\lambda}_d|^2}{L|\bar{\lambda}_p|^2} - \log \left[1 + \frac{(1 + |\alpha|^2|\bar{\lambda}_p|^2\bar{\beta})|\bar{\lambda}_d|^2}{L|\bar{\lambda}_p|^2} \right]$$

Proof: See Appendix H.

Similar to **Proposition 2**, the statistic $\tau(\mathbf{Y}|\mathcal{H}_1)$ is approximated by its first-order expansion $\tilde{\tau}(\mathbf{Y}|\mathcal{H}_1)$. The DP is characterized in the following corollary.

Corollary 3: The DP is given by

$$\mathbb{P}_d = \mathbb{P}(\tau(\mathbf{Y}) > \log \eta | \mathcal{H}_1) = Q_1\left(\sqrt{2a_d}, \sqrt{2b_d}\right), \quad (56)$$

where $Q_1(\cdot)$ denotes the Marcum-Q function of order 1, and

$$a_d = \frac{|\alpha|^2|\bar{\lambda}_p|^2\bar{\beta}}{1 + L^{-1}|\alpha|^2|\bar{\lambda}_d|^2\bar{\beta}},$$

$$b_d = -\log \mathbb{P}_{fa} - \left[|\alpha|^2|\bar{\lambda}_d|^2\bar{\beta} - L \log \left(1 + \frac{|\alpha|^2|\bar{\lambda}_d|^2\bar{\beta}}{L} \right) \right].$$

Proof: See Appendix I.

Remark 4: The result reveals several critical insights into the deterministic-random trade-off in ISAC systems:

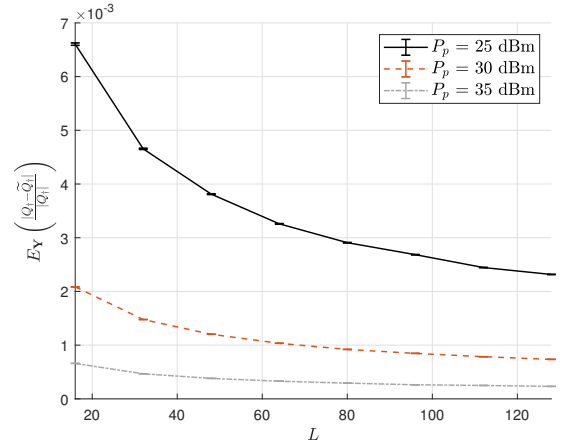


Fig. 3. The relative error of \tilde{Q}_t .

1) **Impact of the Deterministic Component:** Under the GLRT framework, the deterministic component plays a pivotal role in shaping the test statistic. Specifically, the DP monotonically increases with respect to the parameter a_d , which is linearly proportional to the power of deterministic component $|\bar{\lambda}_p|^2$. This implies that as $|\bar{\lambda}_p|^2$ increases, the signal becomes more distinguishable from noise and interference, thereby enhancing the ability to detect the presence of a target. Mathematically, this occurs because the deterministic component contributes directly to the non-centrality parameter of the asymptotic distribution of the test statistic, leading to an increased DP for a fixed threshold.

2) **Impact of the Random Component:** The influence of the random component is more complex. While essential for supporting data transmission, the random component can both help and hinder radar sensing. On one hand, the detection probability decreases with respect to the parameter b_d . Note that $\bar{\beta} \approx \sigma^2 \|P_{\mathbf{V}_d^\perp} \mathbf{a}_t\|^2$, where \mathbf{V}_d^\perp represents the nullspace of clutter, since the CNR is typically large [34]. Thus, a larger $|\bar{\lambda}_d|^2$ leads to a smaller b_d , increasing $|\bar{\lambda}_d|^2$ can improve detection performance by lowering the effective interference in the test statistic. On the other hand, increasing $|\bar{\lambda}_d|^2$ also reduces a_d , which weakens the deterministic component contribution to the test statistic and consequently degrades detection performance.

Remark 5: When $\mathbf{F}_d = \mathbf{0}$, the ISAC system reduces to a conventional radar system that employs only deterministic sensing signals.

$$\tilde{\mathbb{P}}_d = Q_1\left(\sqrt{2|\alpha|^2|\bar{\lambda}_p|^2\bar{\beta}}, \sqrt{-2 \log \mathbb{P}_{fa}}\right), \quad (57)$$

which serves as an theoretical upper bound of DP.

V. SIMULATION RESULTS

In this section, we validate the accuracy of the theoretical analysis and evaluate the performance of the proposed GLRT-based detector through simulations. We consider a millimeter-wave (mmWave) system operating at a carrier frequency of 28 GHz. The transmitter and receiver are equipped with $N = 8$ and $M = 16$ antennas, respectively, and the number of users

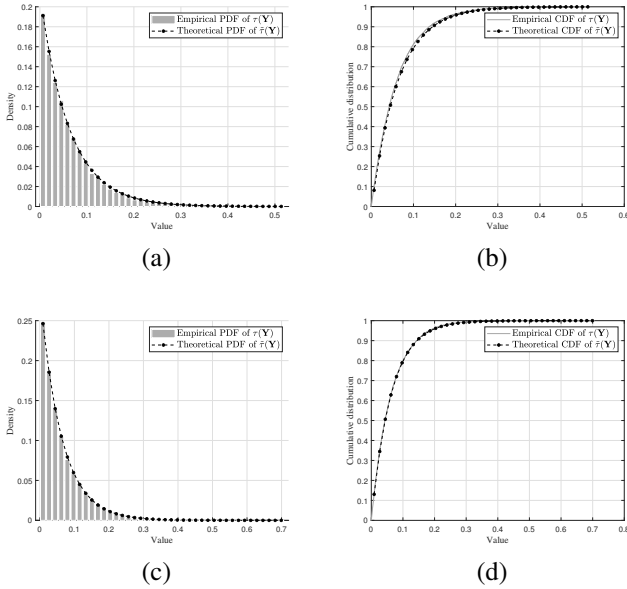


Fig. 4. Histogram distribution function of the $\tau(\mathbf{Y}|\mathcal{H}_0)$ versus $\tilde{\tau}(\mathbf{Y}|\mathcal{H}_0)$, $L = 16$ and $P_d = 30$ dBm. (a) PDF ($P_p = 20$ dBm); (b) CDF ($P_p = 20$ dBm); (c) PDF ($P_p = 30$ dBm); (d) CDF ($P_p = 30$ dBm).

is set to $K = 4$. The clutter channel is modeled according to (5). The path gain for the n -th path is modeled as $\varepsilon_n \sim \mathcal{CN}(0, 10^{-0.1\vartheta(d)})$, where $\vartheta(d) = a + 10b \log_{10}(d) + \epsilon$, with d denoting the propagation distance and $\epsilon \sim \mathcal{CN}(0, \sigma_\epsilon^2)$ [35]. Following the parameter settings in [35], we use $a = 61.4$, $b = 2$, and $\sigma_\epsilon = 5.8$ dB. The distance between the ISAC transmitter and receiver is set as 40 m. The angles of departure (AOD) and arrival (AOA) of the clutter paths are uniformly distributed within the range $[50^\circ, 60^\circ]$. The number of clutter paths is set as $N_{\text{path}} = 3$. We consider one sensing target and 3 communication users whose AOD and AOA are set as 10° and $(20^\circ, 25^\circ, 30^\circ)$, respectively. The noise power is set to $\sigma^2 = -90$ dBm. Unless specified otherwise, the powers of random and deterministic component are set as $P_p = 30$ dBm and $P_d = 30$ dBm, respectively, and $\frac{L_p}{L_d} = \frac{1}{3}$.

A. Approximation Accuracy of the Estimated Unknown Signal Amplitude

The unknown signal amplitude α is estimated by $\alpha_{\dagger} = Q_{\dagger}\gamma$. In **Proposition 1**, we introduce a surrogate of the quantity Q_{\dagger} by its asymptotic approximation \tilde{Q}_{\dagger} . To evaluate the accuracy of this approximation, we first examine the associated approximation error. In particular, we define the relative error as $\Delta_Q = E_{\mathbf{Y}} \left(\frac{|Q_{\dagger} - \tilde{Q}_{\dagger}|}{|Q_{\dagger}|} \right)$, which measures the expectation for the normalized error over the distribution of the observation matrix \mathbf{Y} . Fig. 3 illustrates the relative error for varying values of L . It is observed that the approximation error is small across all considered scenarios, indicating that \tilde{Q}_{\dagger} provides a highly accurate estimate of Q_{\dagger} even for small values of L . Moreover, as L increases, the relative error exhibits a decreasing trend, which agrees with the asymptotic behavior predicted in **Proposition 1**.

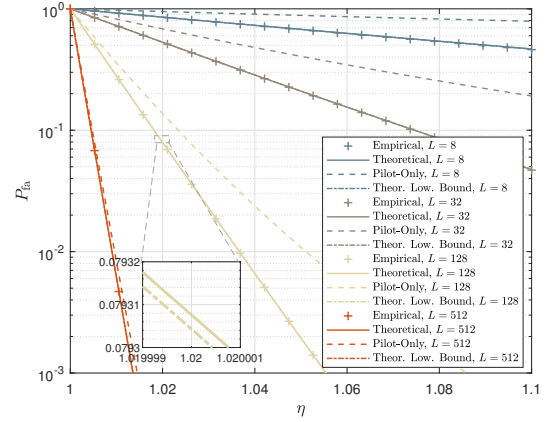


Fig. 5. The FAP \mathbb{P}_{fa} versus η , $P_p = 20$ dBm, and $P_d = 30$ dBm.

B. Approximation Accuracy of Test Statistic $\tilde{\tau}(\mathbf{Y}|\mathcal{H}_0)$

Figs. 4 empirically validates the asymptotic analysis presented in **Proposition 2** with sensing powers $P_p = 20$ dBm and $P_p = 30$ dBm, respectively. Notably, the empirical distribution of the test statistic $\tau(\mathbf{Y}|\mathcal{H}_0)$ aligns closely with the theoretical asymptotic distribution $\tilde{\tau}(\mathbf{Y}|\mathcal{H}_0)$, even when the number of samples is $L = 16$. This result validates the accuracy of the asymptotic analysis in finite-sample regimes. Furthermore, as signal power P_p increases, the empirical and theoretical distributions converge more tightly, especially in the tail regions. This further confirms the accuracy of the proposed asymptotic approximation. This is because, as P_p increases, random fluctuations in the test statistic decrease, yielding less variance in the empirical distribution.

C. False Alarm Probability

Fig. 5 illustrates the FAP as a function of the detection threshold η . The legend “Pilot-Only” represents the FAP of the pilot-only detector in (27) and “Theor. Low. Bound” represents the lower bound of FAP defined in (43). As expected, the FAP decreases with increasing η . Moreover, it is observed that as the number of samples L increases, the theoretical analysis aligns more closely with the empirical FAP. Notably, even for a relatively smaller number of samples, e.g., $L = 4$, the empirical FAP demonstrates a strong agreement with the theoretical value \mathbb{P}_{fa} . As a result, these findings validate the accuracy of the proposed asymptotic expression for the FAP, particularly in practical scenarios where moderately large signal lengths are available.

Moreover, the FAP gap between the proposed detector and the pilot-only detector becomes negligible in the large- L regime (e.g., $L = 512$), as the effect of data payload-induced randomness diminishes with increasing L . However, acquiring a large number of samples introduces higher system latency and computational overhead, which may not be desirable in real-time applications. In contrast, the proposed detector significantly outperforms the pilot-only detector in terms of FAP in the small to moderate- L regime (e.g., $L = 8, 32, 128$). This is because the pilot-only detector ignores the random

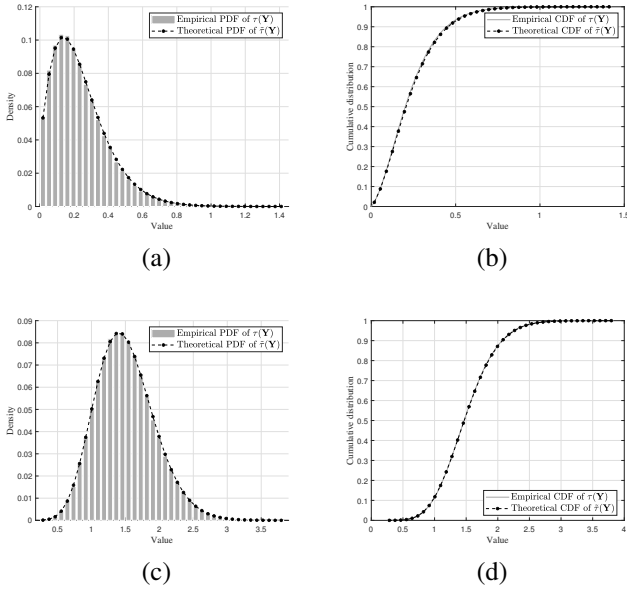


Fig. 6. Histogram distribution function of the $\tau(\mathbf{Y}|\mathcal{H}_1)$ versus $\tilde{\tau}(\mathbf{Y}|\mathcal{H}_1)$, $L = 16$, and $P_d = 30$ dBm. (a) PDF ($P_p = 20$ dBm); (b) CDF ($P_p = 20$ dBm); (c) PDF ($P_p = 30$ dBm); (d) CDF ($P_p = 30$ dBm).

component of the ISAC signal, leading to model mismatch. These results highlight the importance of accounting for data payload-induced randomness in detector design, especially when the number of available samples is limited.

D. Approximation Accuracy of Test Statistic $\tilde{\tau}(\mathbf{Y}|\mathcal{H}_1)$

Figs. 6 offers empirical verification of the asymptotic analysis formulated in **Proposition 3** with $L = 32$ and $L = 128$, respectively. The empirical distribution of $\tau(\mathbf{Y}|\mathcal{H}_1)$ aligns well with its asymptotic counterpart $\tilde{\tau}(\mathbf{Y}|\mathcal{H}_1)$, even for a modest number of samples, i.e., $L = 16$, demonstrating the accuracy of **Proposition 3** in finite-sample regimes. This agreement improves with increasing L , particularly in the tails, confirming the accuracy and practical relevance of the proposed asymptotic formulation.

E. Detection Probability

Fig. 7 shows the receiver operating characteristic (ROC) curves of the proposed GLRT-based detector based on 10,000 Monte Carlo trials. The legend ‘‘Pilot-Only’’ denotes the resultant DP of the pilot-only detector shown in (27) and ‘‘Theor. Up. Bound’’ represents the upper bound of DP defined in (57). As expected, the FAP \mathbb{P}_{fa} increases as the detection threshold η decreases, which improves the detection probability \mathbb{P}_d . The empirical \mathbb{P}_d closely aligns with the theoretical prediction across different L , confirming the accuracy of the asymptotic analysis. Compared to the sensing only detector, the proposed GLRT achieves a better tradeoff between false alarm control and detection ability by explicitly accounting for both deterministic and random components of the ISAC signal. These results highlight the importance of considering the random component in ISAC detector design.

Figure 8 illustrates the impact of the deterministic-random trade-off (DRT) on detection performance. As the sensing

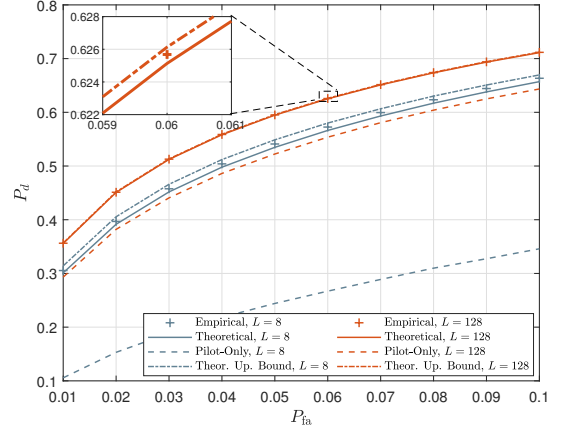


Fig. 7. ROC curve, $P_p = 20$ dBm, and $P_d = 30$ dBm.

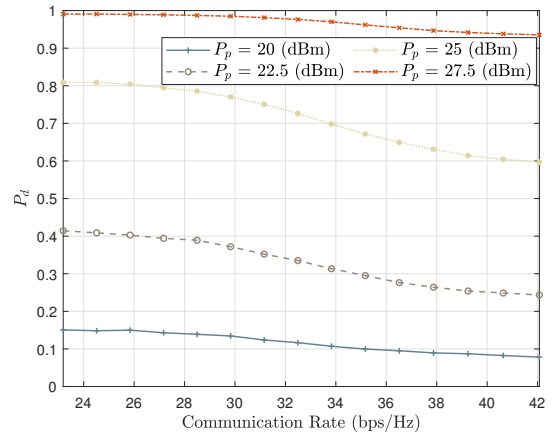


Fig. 8. The DP \mathbb{P}_d versus communication rate, $\mathbb{P}_{fa} = 10^{-3}$, and $L = 2048$.

power P_p increases, the power of the deterministic component also increases, leading to improved DP due to the enhanced known target signature. In contrast, as the communication rate increases, the DP initially drops rapidly and then decreases more slowly. This behavior comes from the random component: while it improves the overall signal signature, it also introduces statistical uncertainty that hinders detection at lower power levels. However, once the power of data payload P_d becomes sufficiently large, the signal enhancement effect of the random component begins to dominate, resulting in a slower decline in DP.

VI. CONCLUSION

The hybrid nature of ISAC signals causes new challenges for target detection due to the coupled shifts in both the mean and variance of the received signal, and the lack of information for the data payloads at the sensing receiver in bistatic configurations. This paper developed a GLRT-based detector to tackle the challenges, where an asymptotic analysis was performed to derive closed-form approximations for FAP and DP. It was shown that the proposed detector achieves reliable target detection performance, and theoretical

$$\begin{aligned}
f'(\alpha) &\triangleq \frac{\partial f(\alpha)}{\partial \alpha^*} \stackrel{(a)}{=} \frac{\alpha |\bar{\lambda}_d|^2}{(1 + |\alpha|^2 |\bar{\lambda}_d|^2 \beta)^2} \text{tr} \left[\boldsymbol{\Sigma}^{-1} \mathbf{a}_t \mathbf{a}_t^H \boldsymbol{\Sigma}^{-1} (\mathbf{Y} - \mathbf{U} - \alpha \lambda_p \mathbf{a}_t \mathbf{s}_p^T \mathbf{J}_p) (\mathbf{Y} - \mathbf{U} - \alpha \lambda_p \mathbf{a}_t \mathbf{s}_p^T \mathbf{J}_p)^H \right] \\
&\quad + \frac{\lambda_p^*}{1 + |\alpha|^2 |\bar{\lambda}_d|^2 \beta} \mathbf{a}_t^H \boldsymbol{\Sigma}^{-1} (\mathbf{Y} - \mathbf{U}) \mathbf{J}_p^T \mathbf{s}_p^* - \frac{\alpha |\lambda_p|^2 \beta}{1 + L |\alpha|^2 |\bar{\lambda}_d|^2 \beta} \|\mathbf{J}_p^T \mathbf{s}_p\|^2 - \frac{\alpha |\bar{\lambda}_d|^2 \beta}{1 + |\alpha|^2 |\bar{\lambda}_d|^2 \beta} \\
&\stackrel{(b)}{=} \frac{\alpha |\bar{\lambda}_d|^2}{(1 + |\alpha|^2 |\bar{\lambda}_d|^2 \beta)^2} \text{tr} \left[\boldsymbol{\Sigma}^{-1} \mathbf{a}_t \mathbf{a}_t^H \boldsymbol{\Sigma}^{-1} (\mathbf{Y} - \mathbf{U} - \alpha \lambda_p \mathbf{a}_t \mathbf{s}_p^T \mathbf{J}_p) (\mathbf{Y} - \mathbf{U} - \alpha \lambda_p \mathbf{a}_t \mathbf{s}_p^T \mathbf{J}_p)^H \right] \\
&\quad + \frac{\lambda_p^* \boldsymbol{\mu}^H \mathbf{J}_p^T \mathbf{s}_p^*}{1 + |\alpha|^2 |\bar{\lambda}_d|^2 \beta} - \frac{\alpha (|\bar{\lambda}_p|^2 + |\bar{\lambda}_d|^2) \beta}{1 + |\alpha|^2 |\bar{\lambda}_d|^2 \beta} \\
&= \frac{\alpha |\bar{\lambda}_d|^2}{(1 + |\alpha|^2 |\bar{\lambda}_d|^2 \beta)^2} (\|\boldsymbol{\mu} - \alpha^* \lambda_p^* \beta \mathbf{J}_p^T \mathbf{s}_p^*\|^2) + \frac{\lambda_p^* \boldsymbol{\mu}^H \mathbf{J}_p^T \mathbf{s}_p^*}{1 + |\alpha|^2 |\bar{\lambda}_d|^2 \beta} - \frac{\alpha (|\bar{\lambda}_p|^2 + |\bar{\lambda}_d|^2) \beta}{1 + |\alpha|^2 |\bar{\lambda}_d|^2 \beta}.
\end{aligned} \tag{58}$$

approximations remain accurate even in finite-sample regimes. An insightful observation regarding target detection by hybrid signals was also obtained: while both deterministic and random components enhance detection reliability, the randomness also introduces statistical uncertainty that may degrade performance. These results highlight the necessity of accounting for data payload-induced randomness in ISAC detector design and provide valuable insights into performance optimization under practical constraints.

APPENDIX A PROOF OF LEMMA 1

Define $f(\alpha) \triangleq \log f_{\mathbf{Y}|\mathcal{H}_1}(\mathbf{Y}; \alpha|\mathcal{H}_1)$. Given the logarithm is monotonic, the main idea of this proof is to find the point α_\dagger such that $f'(\alpha_\dagger) = 0$, where $f'(\alpha)$ denotes the gradient of $f(\alpha)$ with respect to α .

Taking the derivation of $f(\alpha)$ with respect to α yields (58) on the top of this page, where (a) follows the Sherman–Morrison formula, i.e.,

$$\begin{aligned}
(\boldsymbol{\Sigma} + \Delta \boldsymbol{\Sigma}(\alpha))^{-1} \mathbf{a}_t &= (\boldsymbol{\Sigma} + |\alpha|^2 |\bar{\lambda}_d|^2 \mathbf{a}_t \mathbf{a}_t^H)^{-1} \mathbf{a}_t \\
&= \left(\boldsymbol{\Sigma}^{-1} - \frac{|\alpha|^2 |\bar{\lambda}_d|^2 \boldsymbol{\Sigma}^{-1} \mathbf{a}_t \mathbf{a}_t^H \boldsymbol{\Sigma}^{-1}}{1 + |\alpha|^2 |\bar{\lambda}_d|^2 \beta} \right) \mathbf{a}_t \\
&= \left(1 - \frac{|\alpha|^2 |\bar{\lambda}_d|^2 \beta}{1 + |\alpha|^2 |\bar{\lambda}_d|^2 \beta} \right) \boldsymbol{\Sigma}^{-1} \mathbf{a}_t = \frac{\boldsymbol{\Sigma}^{-1} \mathbf{a}_t}{1 + |\alpha|^2 |\bar{\lambda}_d|^2 \beta},
\end{aligned} \tag{59}$$

and (b) follows the constant modulus property of sensing waveform, i.e., $|s_{s,l}| = 1$.

Maximizing the log-likelihood function $f(\alpha)$ by setting $f'(\alpha) = 0$ yields

$$\left[(|\bar{\lambda}_p|^2 + |\bar{\lambda}_d|^2) \beta - \frac{|\bar{\lambda}_d|^2 \|\boldsymbol{\mu} - \alpha^* \lambda_p^* \beta \mathbf{J}_p^T \mathbf{s}_p^*\|^2}{1 + |\alpha|^2 |\bar{\lambda}_d|^2 \beta} \right] \alpha = \gamma. \tag{60}$$

Note that α is a complex number, and (60) is equivalent to a cubic equation in terms of α . Therefore, there are three distinct complex solutions for α , which complicates the problem. Fortunately, we observe that the expression inside the bracket on the left side of the equation is a real number, while alpha and gamma are complex numbers. This implies that the ratio of α to γ is a real number, i.e.,

$$\alpha = Q\gamma, \tag{61}$$

where $Q = \frac{1}{(|\bar{\lambda}_p|^2 + |\bar{\lambda}_d|^2) \beta - \frac{|\bar{\lambda}_d|^2 \|\boldsymbol{\mu} - \alpha^* \lambda_p^* \beta \mathbf{J}_p^T \mathbf{s}_p^*\|^2}{1 + |\alpha|^2 |\bar{\lambda}_d|^2 \beta}}$ is a real number. By substituting (61) into (60), we have

$$aQ^3 + bQ^2 + cQ + d = 0, \tag{62}$$

where

$$\begin{aligned}
a &= |\bar{\lambda}_d|^4 |\gamma|^2 \beta^2, \quad b = |\bar{\lambda}_d|^2 |\gamma|^2 \beta, \\
c &= ((|\bar{\lambda}_p|^2 + |\bar{\lambda}_d|^2) \beta - \|\boldsymbol{\mu}\|^2 |\bar{\lambda}_d|^2) \beta, \quad d = -1.
\end{aligned} \tag{63}$$

Note that (62) is a cubic equation in terms of Q , which has a unique real-valued solution for Q . By applying the Cardano formula, the unique real-valued solution is provided by

$$Q_\dagger = -\frac{b}{3a} + \sqrt[3]{\Delta_1 + \sqrt{\Delta_1^2 + \Delta_2^3}} + \sqrt[3]{\Delta_1 - \sqrt{\Delta_1^2 + \Delta_2^3}},$$

where $\Delta_1 = \frac{bc}{6a^2} - \frac{b^3}{27a^3} - \frac{d}{2a}$ and $\Delta_2 = \frac{c}{3a} - \frac{b^2}{9a^2}$.

APPENDIX B PROOF OF LEMMA 2

The quantity $\frac{\|\bar{\boldsymbol{\mu}}\|^2}{\beta}$ can be expressed as the sum of the squared magnitudes of the terms $\frac{\mathbf{a}_t^H \boldsymbol{\Sigma}^{-1/2} \mathbf{z}_l}{\sqrt{\beta}}$, for $l = 1, 2, \dots, L$, i.e.,

$$\frac{\|\bar{\boldsymbol{\mu}}\|^2}{\beta} = \sum_{l=1}^L \left| \frac{\mathbf{a}_t^H \boldsymbol{\Sigma}^{-1/2} \mathbf{z}_l}{\sqrt{\beta}} \right|^2, \tag{64}$$

where \mathbf{z}_l denotes the l -th column of the matrix \mathbf{Z} . Note that the elements of vector \mathbf{z}_l are i.i.d. Gaussian random variables, and the term $\frac{\mathbf{a}_t^H \boldsymbol{\Sigma}^{-1/2} \mathbf{z}_l}{\sqrt{\beta}}$ is a linear combination of these elements.

It thus follows from the closure property of multivariate Gaussian distributions under linear transformations that such term is itself a Gaussian random variable. Consequently, $\frac{\|\bar{\boldsymbol{\mu}}\|^2}{\beta}$ is the sum of the squared magnitudes of L independent Gaussian random variables with mean 0 and variance 1. It indicates that $\frac{2\|\bar{\boldsymbol{\mu}}\|^2}{\beta}$ follows the Chi-square distribution with $2L$ complex degree of freedom, whose mean and variance are $2L$ and $4L$, respectively. Therefore, the mean and variance of $\frac{\|\bar{\boldsymbol{\mu}}\|^2}{\beta}$ are respectively given by

$$\mathbb{E} \left(\frac{\|\bar{\boldsymbol{\mu}}\|^2}{\beta} \right) = L^{-1} \mathbb{E} \left(\frac{\|\bar{\boldsymbol{\mu}}\|^2}{\beta} \right) = 1, \tag{65}$$

$$\text{var} \left(\frac{\|\boldsymbol{\mu}\|^2}{\beta} \right) = L^{-2} \text{var} \left(\frac{\|\bar{\boldsymbol{\mu}}\|^2}{\beta} \right) = L^{-1}. \quad (66)$$

Then, according to the Chebyshev's inequality, for any real number $\epsilon > 0$

$$\mathbb{P} \left(L^{\frac{1}{2}-\delta} \left| \frac{\|\boldsymbol{\mu}\|^2}{\beta} - 1 \right| \geq \epsilon \right) \leq \frac{L^{1-2\delta} \text{var} \left(\frac{\|\boldsymbol{\mu}\|^2}{\beta} \right)}{\epsilon^2} \xrightarrow{\text{a.s.}} 0, \quad (67)$$

which completes the proof.

APPENDIX C PROOF OF LEMMA 3

Recalling the definition of γ in (19), we have

$$\begin{aligned} \gamma &= \lambda_p^* \mathbf{a}_t^H \boldsymbol{\Sigma}^{-1} (\mathbf{Y} - \mathbf{U}) \mathbf{J}_p^T \mathbf{s}_p^* \\ &= L^{-1} \lambda_p^* \mathbf{a}_t^H \bar{\boldsymbol{\Sigma}}^{-\frac{1}{2}} \mathbf{Z} \mathbf{J}_p^T \mathbf{s}_p^* \\ &= L^{-1} \lambda_p^* \sum_{i=1}^N \sum_{j=1}^L \left[\bar{\boldsymbol{\Sigma}}^{-\frac{1}{2}} \mathbf{a}_t \right]_i \left[\mathbf{J}_p^T \mathbf{s}_p^* \right]_j W_{i,j}, \end{aligned} \quad (68)$$

where $[\mathbf{a}]_i$ denotes the i th entry of the vector \mathbf{a} , and $W_{i,j}$ denotes the (i, j) th entry of \mathbf{Z} . This expression shows that γ is a linear combination of the entries of \mathbf{Z} , weighted by deterministic coefficients determined by system parameters.

Since the entries of \mathbf{Z} are assumed to be independent and identically distributed (i.i.d.) complex Gaussian random variables with zero mean and unit variance, it follows that γ is also a complex Gaussian random variable with zero mean. The variance of γ is determined by the squared magnitudes of the corresponding weights in the summation, yielding

$$\begin{aligned} \text{var}(\gamma) &= L^{-2} |\lambda_p|^2 \sum_{i=1}^N \sum_{j=1}^L \left| \left[\bar{\boldsymbol{\Sigma}}^{-1/2} \mathbf{a}_t \right]_i \right|^2 \left| \left[\mathbf{J}_p^T \mathbf{s}_p^* \right]_j \right|^2 \\ &= L^{-2} |\bar{\lambda}_p|^2 \bar{\beta}, \end{aligned} \quad (69)$$

where (a) follows from $\|\mathbf{s}_p\|^2 = L_p$ and $\left\| \bar{\boldsymbol{\Sigma}}^{-1/2} \mathbf{a}_t \right\|^2 = \bar{\beta}$. Therefore, $\Gamma \triangleq |\gamma|^2$ follows a Gamma distribution with a shape parameter 1 and a scale parameter $L^{-2} |\bar{\lambda}_p|^2 \bar{\beta}$. Its mean and variance are respectively given by

$$\mu_\Gamma = \mathbb{E}(\Gamma) = L^{-2} |\bar{\lambda}_p|^2 \bar{\beta}, \quad (70)$$

$$\sigma_\Gamma^2 = \text{var}(\Gamma) = L^{-4} |\bar{\lambda}_p|^4 \bar{\beta}^2. \quad (71)$$

According to the Markov's inequality, for any real number $\delta, \epsilon > 0$, and any positive integer p , we have

$$\begin{aligned} \mathbb{P} \left(L^{2p-\epsilon} |\Gamma - \mu_\Gamma|^p \geq \delta \right) &= \mathbb{P} \left(L^{2-\frac{\epsilon}{p}} |\Gamma - \mu_\Gamma| \geq \sqrt[p]{\delta} \right) \\ &\leq \frac{L^{2-\frac{\epsilon}{p}} \mu_\Gamma}{\sqrt[p]{\delta}} = \frac{L^{-\frac{\epsilon}{p}} |\bar{\lambda}_p|^2 \bar{\beta}}{\sqrt[p]{\delta}} \xrightarrow{\text{a.s.}} 0. \end{aligned} \quad (72)$$

This result immediately implies that, $\forall \epsilon > 0$,

$$\sup_{\mathbf{Y}} L^{2p-\epsilon} |\Gamma - \mu_\Gamma|^p \xrightarrow{\text{a.s.}} 0, \quad (73)$$

which indicates that the scaled deviation $|\Gamma - \mu_\Gamma|^p$ fluctuates at the order of L^{-2p} . Consequently, for any $\xi \in (0, \epsilon)$, there exists a sufficiently large L such that, a.s.,

$$|\Gamma - \mu_\Gamma|^p = \mathcal{O}(L^{-2p}), \quad (74)$$

which completes the proof.

APPENDIX D PROOF OF PROPOSITION 1

The main idea of this proof is to demonstrate that, in the asymptotic regime, Q_\dagger is the solution to the equation:

$$L^{-1} |\bar{\lambda}_p|^2 \bar{\beta} Q - 1 = 0. \quad (75)$$

Recalling the proof in *Appendix A*, Q_\dagger is the solution to the equation in (62). Based on the definition in (32), the coefficients in can be reformulated by

$$\begin{aligned} a &= L^{-4} |\bar{\lambda}_d|^4 |\bar{\gamma}|^2 \bar{\beta}^2, \quad b = L^{-3} |\bar{\lambda}_d|^2 |\bar{\gamma}|^2 \bar{\beta}, \\ c &= L^{-1} \left((|\bar{\lambda}_p|^2 + |\bar{\lambda}_d|^2) \bar{\beta} - L^{-1} \|\bar{\boldsymbol{\mu}}\|^2 |\bar{\lambda}_d|^2 \right). \end{aligned} \quad (76)$$

Assume that $Q = CL^p$, where C denotes a finite constant independent of L . Then, (62) can be reformulated as

$$\begin{aligned} C^3 L^{3p-4} |\bar{\lambda}_d|^4 |\bar{\gamma}|^2 \bar{\beta}^2 + C^2 L^{2p-3} |\bar{\lambda}_d|^2 |\bar{\gamma}|^2 \bar{\beta} + \\ C L^{p-1} \left((|\bar{\lambda}_p|^2 + |\bar{\lambda}_d|^2) \bar{\beta} - L^{-1} \|\bar{\boldsymbol{\mu}}\|^2 |\bar{\lambda}_d|^2 \right) - 1 = 0. \end{aligned} \quad (77)$$

The condition for this equation to be solvable is $\{3p-4 \leq 0, 2p-3 \leq 0, p-1 \leq 0\}$, which is equivalent to $p \leq 1$. Then, we have $L^{3p-4} \ll L^{p-1}$ and $L^{2p-3} \ll L^{p-1}$. Thus, aQ^3 and bQ^2 can be omitted and (77) is equivalent to

$$cQ - 1 = 0. \quad (78)$$

Meanwhile, by invoking *Lemma 2*, we have

$$\begin{aligned} c &= \frac{1}{Q} = L^{-1} |\bar{\lambda}_p|^2 \bar{\beta} - L^{-1} |\bar{\lambda}_d|^2 \left(L^{-1} \|\bar{\boldsymbol{\mu}}\|^2 - \bar{\beta} \right) \\ &= L^{-1} |\bar{\lambda}_p|^2 \bar{\beta} + \mathcal{O} \left(L^{-\frac{3}{2}} \right). \end{aligned} \quad (79)$$

It follows that $Q_\dagger = \frac{1}{L^{-1} |\bar{\lambda}_p|^2 \bar{\beta}}$.

APPENDIX E PROOF OF PROPOSITION 2

This proof consists of three steps:

1) **Decomposition of τ** : First, we show that

$$\tau(\mathbf{Y}) \xrightarrow{\text{a.s.}} g(\Gamma) - h(\Gamma), \quad (80)$$

where

$$g(\Gamma) = \frac{(\rho_d + \rho_p)\Gamma}{1 + \rho_d\Gamma}, \quad h(\Gamma) = \log(1 + \rho_d\Gamma), \quad (81)$$

with

$$\rho_d = L^{-1} Q_\dagger^2 |\bar{\lambda}_d|^2 \bar{\beta} = \frac{L |\bar{\lambda}_d|^2}{|\bar{\lambda}_p|^4 \bar{\beta}}, \quad (82)$$

$$\rho_p = L^{-1} Q_\dagger^2 |\bar{\lambda}_p|^2 \bar{\beta} = \frac{L}{|\bar{\lambda}_p|^2 \bar{\beta}}. \quad (83)$$

The purpose of this decomposition is to simplify the notation and facilitate the asymptotic analysis.

2) **Asymptotic approximation of $g(\Gamma)$** : Next, we analyze the asymptotic behavior of $g(\Gamma)$ and show that, as $L \rightarrow \infty$,

$$g(\Gamma) \xrightarrow{\text{a.s.}} \frac{(\rho_d + \rho_p)\mu_\Gamma}{1 + \rho_d\mu_\Gamma} + \frac{(\rho_d + \rho_p)(\Gamma - \mu_\Gamma)}{(1 + \rho_d\mu_\Gamma)^2}, \quad (84)$$

3) **Asymptotic approximation of $h(\Gamma)$:** Then, we prove that, as $L \rightarrow \infty$,

$$h(\Gamma) \stackrel{a.s.}{\rightarrow} \log(1 + \rho_d \mu_\Gamma) + \frac{\rho_d (\Gamma - \mu_\Gamma)}{1 + \rho_d \mu_\Gamma}. \quad (85)$$

4) **Rearrangement of $g(\Gamma) - h(\Gamma)$:** Finally, we prove that

$$\tau(\mathbf{Y}) = \varrho_0 |\gamma|^2 + \zeta_0. \quad (86)$$

The following outlines the detailed steps involved:

1) Recalling (26), we have

$$\tau(\mathbf{Y}) = \tau_1 + \tau_2 + \tau_3 - h(\Gamma), \quad (87)$$

where

$$\begin{aligned} \tau_1 &= \frac{Q_\dagger^2 |\bar{\lambda}_d|^2 |\gamma|^2 \|\boldsymbol{\mu}\|^2}{1 + Q_\dagger^2 |\bar{\lambda}_d|^2 |\gamma|^2 \beta}, \tau_2 = \frac{2Q_\dagger |\gamma|^2}{1 + Q_\dagger^2 |\bar{\lambda}_d|^2 |\gamma|^2 \beta}, \\ \tau_3 &= -\frac{Q_\dagger^2 |\bar{\lambda}_p|^2 |\gamma|^2 \beta}{1 + Q_\dagger^2 |\bar{\lambda}_d|^2 |\gamma|^2 \beta}. \end{aligned} \quad (88)$$

By invoking the approximation of Q_\dagger provided in (38), the expression of τ_2 simplifies to

$$\tau_2 = \frac{2L^{-1} Q_\dagger^2 |\bar{\lambda}_p|^2 |\gamma|^2 \bar{\beta}}{1 + L^{-1} Q_\dagger^2 |\bar{\lambda}_d|^2 |\gamma|^2 \bar{\beta}}. \quad (89)$$

Accordingly, the sum of τ_1 , τ_2 , and τ_3 , denoted by $g(\Gamma)$, is given by

$$\begin{aligned} g(\Gamma) &= \frac{L^{-1} Q_\dagger^2 \left(\frac{\|\boldsymbol{\mu}\|^2}{\beta} |\bar{\lambda}_d|^2 + |\bar{\lambda}_p|^2 \right) |\gamma|^2 \bar{\beta}}{1 + L^{-1} Q_\dagger^2 |\bar{\lambda}_d|^2 |\gamma|^2 \bar{\beta}} \\ &\stackrel{(a)}{=} \frac{L^{-1} Q_\dagger^2 (|\bar{\lambda}_d|^2 + |\bar{\lambda}_p|^2) |\gamma|^2 \bar{\beta}}{1 + L^{-1} Q_\dagger^2 |\bar{\lambda}_d|^2 |\gamma|^2 \bar{\beta}} = \frac{(\rho_d + \rho_p) \Gamma}{1 + \rho_d \Gamma}, \end{aligned} \quad (90)$$

where (a) follows from **Lemma 2**.

2) The main idea of this paper is to show that, the first- and second-order terms in the Taylor expansion of $g(\Gamma)$ with respect to μ_Γ contribute fluctuations of order $\mathcal{O}(L^{-1})$, while the remainder terms are asymptotically negligible, with magnitude bounded by $\mathcal{O}(L^{-3})$ or smaller.

First, by applying the first-order Taylor expansion of $g(\Gamma)$ about the point $\Gamma = \mu_\Gamma$, we obtain

$$\begin{aligned} g(\Gamma) &= g(\mu_\Gamma) + \sum_{i=1}^{\infty} \frac{g^{(i)}(\mu_\Gamma)}{i!} (\Gamma - \mu_\Gamma)^i \\ &= \frac{(\rho_d + \rho_p) \mu_\Gamma}{1 + \rho_d \mu_\Gamma} + \frac{(\rho_d + \rho_p) (\Gamma - \mu_\Gamma)}{(1 + \rho_d \mu_\Gamma)^2} \\ &\quad + \sum_{i=2}^{\infty} \frac{(-1)^{i-1} (\rho_d + \rho_p) \rho_d^{i-1}}{(1 + \rho_d \mu_\Gamma)^{i+1}} (\Gamma - \mu_\Gamma)^i, \end{aligned} \quad (91)$$

where $g^{(i)}(\mu_\Gamma)$ denotes the i th derivative of $g(\cdot)$ with respect to γ evaluated at the point μ_Γ . Note that $\rho_d = \frac{L |\bar{\lambda}_d|^2}{|\bar{\lambda}_p|^4 \bar{\beta}}$ and $\rho_p = \frac{L}{|\bar{\lambda}_p|^2 \bar{\beta}}$ fluctuate at the order of L^1 . Also, according to **Lemma 3**, both μ_Γ and $|\Gamma - \mu_\Gamma|$ fluctuate at the order of L^{-2} , i.e., $\mu_\Gamma = \mathcal{O}(L^{-2})$, and $|\Gamma - \mu_\Gamma| = \mathcal{O}(L^{-2})$. It follows that the first two terms in $g(\Gamma)$ fluctuate at the order of L^{-1} . Moreover, it holds that

$$\left| \frac{(-1)^{i-1} (\rho_d + \rho_p) \rho_d^{i-1}}{(1 + \rho_d \mu_\Gamma)^{i+1}} (\Gamma - \mu_\Gamma)^i \right| = \mathcal{O}(L^{-i}). \quad (92)$$

Thus, we conclude that $g(\Gamma)$ can be accurately represented by the truncated expansion retaining the dominant two terms, i.e.,

$$g(\Gamma) = \frac{(\rho_d + \rho_p) \mu_\Gamma}{1 + \rho_d \mu_\Gamma} + \frac{(\rho_d + \rho_p) (\Gamma - \mu_\Gamma)}{(1 + \rho_d \mu_\Gamma)^2} + \mathcal{O}(L^{-2}). \quad (93)$$

3) Similar to the second part, the primary objective of this proof is to demonstrate that the first- and second-order terms in the Taylor expansion of $h(\Gamma)$ exhibit fluctuations of order L^{-1} , whereas all higher-order terms are asymptotically negligible, exhibiting fluctuations of order L^{-2} or smaller.

By expanding $h(\Gamma)$ at the point $\Gamma = \mu_\Gamma$, we first observe that

$$\begin{aligned} h(\Gamma) &= h(\mu_\Gamma) + \sum_{i=1}^{\infty} \frac{h^{(i)}(\mu_\Gamma)}{i!} (\Gamma - \mu_\Gamma)^i \\ &= \log(1 + \rho_d \mu_\Gamma) + \frac{\rho_d (\Gamma - \mu_\Gamma)}{1 + \rho_d \mu_\Gamma} \\ &\quad + \sum_{i=2}^{\infty} \frac{(-1)^{i-1}}{i} \left(\frac{\rho_d}{1 + \rho_d \mu_\Gamma} \right)^i (\Gamma - \mu_\Gamma)^i. \end{aligned} \quad (94)$$

Note that $\rho_d = \mathcal{O}(L)$. Then, according to **Lemma 3**, we have

$$\begin{aligned} &\left| \sum_{i=2}^{\infty} (-1)^{i-1} \left(\frac{\rho_d}{1 + \rho_d \mu_\Gamma} \right)^i (\Gamma - \mu_\Gamma)^i \right| \\ &\leq \sum_{i=2}^{\infty} \left(\frac{\rho_d}{1 + \rho_d \mu_\Gamma} \right)^i |\Gamma - \mu_\Gamma|^i = \mathcal{O}(L^{-2}). \end{aligned} \quad (95)$$

Since $\rho_d \mu_\Gamma = \mathcal{O}(L^{-1})$, according to the L'Hopital's rule, we have

$$\log(1 + \rho_d \mu_\Gamma) \stackrel{a.s.}{\rightarrow} \rho_d \mu_\Gamma = \mathcal{O}(L^{-1}). \quad (96)$$

Thus, $h(\Gamma)$ can be accurately represented by truncating its Taylor expansion after the second term, i.e.,

$$h(\Gamma) \stackrel{a.s.}{\rightarrow} \log(1 + \rho_d \mu_\Gamma) + \frac{\rho_d (\Gamma - \mu_\Gamma)}{1 + \rho_d \mu_\Gamma} + \mathcal{O}(L^{-2}), \quad (97)$$

which is exactly (85).

4) By rearranging $g(\Gamma) + h(\Gamma)$, we have

$$\begin{aligned} \varrho_0 &= \frac{(\rho_d + \rho_p)}{(1 + \rho_d \mu_\Gamma)^2} - \frac{\rho_d}{1 + \rho_d \mu_\Gamma} = \frac{\rho_p - \rho_d^2 \mu_\Gamma}{(1 + \rho_d \mu_\Gamma)^2} \\ &= \frac{1}{L^{-1} |\bar{\lambda}_p|^2 \bar{\beta}} \cdot \frac{\left(1 - \frac{|\bar{\lambda}_d|^4}{L |\bar{\lambda}_p|^4}\right)}{\left(1 + \frac{|\bar{\lambda}_d|^2}{L |\bar{\lambda}_p|^2}\right)^2} \approx \frac{L}{|\bar{\lambda}_p|^2 \bar{\beta}}, \end{aligned} \quad (98)$$

$$\begin{aligned} \zeta_0 &= \frac{(\rho_d + \rho_p) \mu_\Gamma}{1 + \rho_d \mu_\Gamma} - \frac{(\rho_d + \rho_p) \mu_\Gamma}{(1 + \rho_d \mu_\Gamma)^2} + \frac{\rho_d \mu_\Gamma}{1 + \rho_d \mu_\Gamma} - \log(1 + \rho_d \mu_\Gamma) \\ &= \frac{|\bar{\lambda}_d|^2}{L |\bar{\lambda}_p|^2} \cdot \frac{\left[2 \frac{|\bar{\lambda}_d|^2}{L |\bar{\lambda}_p|^2} + \frac{1}{L} + 1\right]}{\left(1 + \frac{|\bar{\lambda}_d|^2}{L |\bar{\lambda}_p|^2}\right)^2} - \log\left(1 + \frac{|\bar{\lambda}_d|^2}{L |\bar{\lambda}_p|^2}\right) \\ &\approx \frac{|\bar{\lambda}_d|^2}{L |\bar{\lambda}_p|^2} - \log\left(1 + \frac{|\bar{\lambda}_d|^2}{L |\bar{\lambda}_p|^2}\right). \end{aligned} \quad (99)$$

APPENDIX F
PROOF OF LEMMA 4

By invoking (46) into (19b), we have, under \mathcal{H}_1 ,

$$\bar{\boldsymbol{\mu}} = \alpha \lambda_p^* \bar{\beta} \mathbf{J}_p^T \mathbf{s}_p^* + \mathbf{Z}^H (\bar{\boldsymbol{\Sigma}} + \Delta \bar{\boldsymbol{\Sigma}}(\alpha))^{\frac{1}{2}} \bar{\boldsymbol{\Sigma}}^{-1} \mathbf{a}_t. \quad (100)$$

and the l th entry of $\bar{\boldsymbol{\mu}}$ is given by

$$[\bar{\boldsymbol{\mu}}]_l = \alpha \lambda_p^* \bar{\beta} [\mathbf{J}_p^T \mathbf{s}_p^*]_l + \mathbf{z}_l^H (\bar{\boldsymbol{\Sigma}} + \Delta \bar{\boldsymbol{\Sigma}}(\alpha))^{\frac{1}{2}} \bar{\boldsymbol{\Sigma}}^{-1} \mathbf{a}_t, \quad (101)$$

where \mathbf{z}_l denotes the l -th column of the matrix \mathbf{Z} . Given α is a deterministic but unknown parameter, we have

$$\mathbb{E}([\bar{\boldsymbol{\mu}}]_l) = \alpha \lambda_p^* \bar{\beta} [\mathbf{J}_p^T \mathbf{s}_p^*]_l, \quad (102)$$

$$\text{var}([\bar{\boldsymbol{\mu}}]_l) = \mathbb{E}(|[\bar{\boldsymbol{\mu}}]_l - \mathbb{E}([\bar{\boldsymbol{\mu}}]_l)|^2) = \kappa \bar{\beta}. \quad (103)$$

Note that $|[\bar{\boldsymbol{\mu}}]_l|^2 / \left(\frac{\text{var}([\bar{\boldsymbol{\mu}}]_l)}{2}\right)$ follows a non-central chi-square distribution with 2 degrees of freedom (DOF) and non-central parameter $2\kappa^{-1}|\alpha|^2|\lambda_p|^2\bar{\beta}|[\mathbf{J}_p^T \mathbf{s}_p^*]_l|^2$, i.e.,

$$\frac{|[\bar{\boldsymbol{\mu}}]_l|^2}{\frac{\text{var}([\bar{\boldsymbol{\mu}}]_l)}{2}} \sim \chi_2^2 \left(2\kappa^{-1}|\alpha|^2|\lambda_p|^2\bar{\beta} \left| [\mathbf{J}_p^T \mathbf{s}_p^*]_l \right|^2 \right). \quad (104)$$

Therefore, we have

$$\frac{2\kappa^{-1}||\bar{\boldsymbol{\mu}}||^2}{\bar{\beta}} \sim \chi_{2L}^2 (2\kappa^{-1}|\alpha|^2|\bar{\lambda}_p|^2\bar{\beta}). \quad (105)$$

It follows that, the mean and variance of $\frac{||\bar{\boldsymbol{\mu}}||^2}{\bar{\beta}}$ are respectively given by

$$\begin{aligned} \mathbb{E}\left(\frac{||\bar{\boldsymbol{\mu}}||^2}{\bar{\beta}}\right) &= L\kappa + |\alpha|^2|\bar{\lambda}_p|^2\bar{\beta}, \\ \text{var}\left(\frac{||\bar{\boldsymbol{\mu}}||^2}{\bar{\beta}}\right) &= L\kappa^2 + 2\kappa|\alpha|^2|\bar{\lambda}_p|^2\bar{\beta}. \end{aligned} \quad (106)$$

Thus, we have

$$\begin{aligned} \hat{\mu} &\triangleq \mathbb{E}\left(\frac{||\boldsymbol{\mu}||^2}{\beta}\right) = L^{-1}\mathbb{E}\left(\frac{||\bar{\boldsymbol{\mu}}||^2}{\bar{\beta}}\right) \\ &= 1 + L^{-1}|\alpha|^2(|\bar{\lambda}_p|^2 + |\bar{\lambda}_d|^2)\bar{\beta} = 1 + \mathcal{O}(L^{-1}), \end{aligned}$$

and

$$\begin{aligned} \sigma_W^2 &\triangleq \text{var}\left(\frac{||\boldsymbol{\mu}||^2}{\beta}\right) = L^{-2}\text{var}\left(\frac{||\bar{\boldsymbol{\mu}}||^2}{\bar{\beta}}\right) \\ &= L^{-1}(\kappa^2 + 2L^{-1}\kappa|\alpha|^2|\bar{\lambda}_p|^2\bar{\beta}) = \kappa^2 L^{-1} + \mathcal{O}(L^{-2}). \end{aligned}$$

Then, according to the Chebyshev's inequality, for any real number $\epsilon > 0$

$$\mathbb{P}\left(L^{\frac{1}{2}-\delta} \left| \frac{||\boldsymbol{\mu}||^2}{\beta} - \hat{\mu} \right| \geq \epsilon\right) \leq \frac{L^{1-2\delta}\sigma_W^2}{\epsilon^2} \xrightarrow[L \rightarrow \infty]{a.s.} 0. \quad (107)$$

APPENDIX G
PROOF OF LEMMA 5

Define

$$\bar{\gamma} \triangleq \lambda_p^* \bar{\boldsymbol{\mu}}^H \mathbf{J}_p^T \mathbf{s}_p^*. \quad (108)$$

By invoking (46) into (19c), we have, under \mathcal{H}_1 ,

$$\bar{\gamma} = L\alpha^*|\lambda_p|^2\bar{\beta} + \lambda_p^* \mathbf{a}_t^H \bar{\boldsymbol{\Sigma}}^{-1} (\bar{\boldsymbol{\Sigma}} + \Delta \bar{\boldsymbol{\Sigma}}(\alpha))^{\frac{1}{2}} \mathbf{Z} \mathbf{J}_p^T \mathbf{s}_p^*. \quad (109)$$

Then, we have $\mathbb{E}(\bar{\gamma}) = L\alpha^*|\lambda_p|^2\bar{\beta}$, and

$$\begin{aligned} \text{var}(\bar{\gamma}) &= \mathbb{E}(|\bar{\gamma} - \mathbb{E}(\bar{\gamma})|^2) \\ &\stackrel{(a)}{=} |\lambda_p|^2 \sum_{i=1}^N \sum_{j=1}^L \left| \left[\mathbf{a}_t^H \bar{\boldsymbol{\Sigma}}^{-1} (\bar{\boldsymbol{\Sigma}} + \Delta \bar{\boldsymbol{\Sigma}}(\alpha))^{\frac{1}{2}} \right]_i \right|^2 \left| [\mathbf{J}_p^T \mathbf{s}_p^*]_j \right|^2 \\ &= |\bar{\lambda}_p|^2 \bar{\beta} \kappa, \end{aligned}$$

where (a) follows from the property that $W_{i,j}$ are i.i.d. zero-mean unit-variance complex Gaussian random variables, i.e.,

$$\mathbb{E}(W_{i,j} W_{m,n}^*) = \begin{cases} 1, & i = m, j = n, \\ 0, & \text{otherwise.} \end{cases} \quad (110)$$

Then, we have $\frac{|\bar{\gamma}|^2}{\text{var}(\bar{\gamma})} \sim \chi_2^2 \left(\frac{2|\alpha|^2|\bar{\lambda}_p|^2\bar{\beta}}{\kappa} \right)$. It follows that

$$\mathbb{E}\left(\frac{|\bar{\gamma}|^2}{\text{var}(\bar{\gamma})}\right) = 1 + \frac{|\alpha|^2|\bar{\lambda}_p|^2\bar{\beta}}{\kappa}, \quad (111)$$

$$\text{var}\left(\frac{|\bar{\gamma}|^2}{\text{var}(\bar{\gamma})}\right) = 1 + \frac{2|\alpha|^2|\bar{\lambda}_p|^2\bar{\beta}}{\kappa}. \quad (112)$$

Therefore, we have

$$\begin{aligned} \mathbb{E}(|\gamma|^2) &= L^{-2}\mathbb{E}(|\bar{\gamma}|^2) = \frac{\text{var}(\bar{\gamma})}{L^2} \mathbb{E}\left(\frac{|\bar{\gamma}|^2}{\text{var}(\bar{\gamma})}\right) \\ &= L^{-2}\kappa|\bar{\lambda}_p|^2\bar{\beta} + L^{-2}|\alpha|^2|\bar{\lambda}_p|^4\bar{\beta}^2, \end{aligned} \quad (113)$$

$$\begin{aligned} \text{var}(|\gamma|^2) &= L^{-4}\text{var}(|\bar{\gamma}|^2) = \frac{\text{var}^2(\bar{\gamma})}{L^4} \text{var}\left(\frac{|\bar{\gamma}|^2}{\text{var}(\bar{\gamma})}\right) \\ &= L^{-4}\kappa^2|\bar{\lambda}_p|^4\bar{\beta}^2 + 2L^{-4}\kappa|\alpha|^2|\bar{\lambda}_p|^6\bar{\beta}^3. \end{aligned} \quad (114)$$

Then, according to the Chebyshev's inequality, for any real number $\epsilon > 0$

$$\begin{aligned} \mathbb{P}(L^{2-\delta} ||\gamma|^2 - \mathbb{E}(|\gamma|^2)| \geq \epsilon) &\leq \frac{L^{4-2\delta} \cdot \text{var}(|\gamma|^2)}{\epsilon^2} \\ &\leq \frac{L^{-2\delta} (\kappa^2|\bar{\lambda}_p|^4\bar{\beta}^2 + 2\kappa|\alpha|^2|\bar{\lambda}_p|^6\bar{\beta}^3)}{\epsilon^2} \xrightarrow[L \rightarrow \infty]{a.s.} 0. \end{aligned} \quad (115)$$

APPENDIX H
PROOF OF PROPOSITION 3

Similar to the proof in *Appendix E*, the detector in \mathcal{H}_1 is approximated to

$$\begin{aligned} \tau(\mathbf{Y}) &= \frac{\kappa(\rho_d + \rho_p)\mu_\Gamma}{1 + \rho_d\mu_\Gamma} + \frac{\kappa(\rho_d + \rho_p)(\Gamma - \mu_\Gamma)}{(1 + \rho_d\mu_\Gamma)^2} \\ &\quad - \log(1 + \rho_d\mu_\Gamma) - \frac{\rho_d(\Gamma - \mu_\Gamma)}{1 + \rho_d\mu_\Gamma}. \end{aligned} \quad (116)$$

Recalling (49), we have $\kappa = 1 + \mathcal{O}(L^{-1})$. Then, by rearranging (116), we have

$$\varrho_1 \approx \frac{L}{|\bar{\lambda}_p|^2\bar{\beta}} \cdot \frac{\left(1 - \frac{|\bar{\lambda}_d|^4}{L|\bar{\lambda}_p|^4} (1 + |\alpha|^2|\bar{\lambda}_p|^2\bar{\beta})\right)}{\left(1 + \frac{|\bar{\lambda}_d|^2}{L|\bar{\lambda}_p|^2} (1 + |\alpha|^2|\bar{\lambda}_p|^2\bar{\beta})\right)^2} \approx \frac{L}{|\bar{\lambda}_p|^2\bar{\beta}},$$

$$\zeta_1 \approx \frac{(1 + |\alpha|^2 |\bar{\lambda}_p|^2 \bar{\beta}) |\bar{\lambda}_d|^2}{L |\bar{\lambda}_p|^2} - \log \left[1 + \frac{(1 + |\alpha|^2 |\bar{\lambda}_p|^2 \bar{\beta}) |\bar{\lambda}_d|^2}{L |\bar{\lambda}_p|^2} \right] \quad [14]$$

APPENDIX I

PROOF OF COROLLARY 3

Since $\frac{|\bar{\gamma}|^2}{\text{var}(\bar{\gamma})/2}$ follows the non-central Chi-square distribution with degrees of freedom 2 and non-centrality parameter $\frac{2|\alpha|^2 |\bar{\lambda}_p|^2 \bar{\beta}}{1 + L^{-1} |\alpha|^2 |\bar{\lambda}_d|^2 \bar{\beta}}$, we have

$$\begin{aligned} \mathbb{P}_d &= \mathbb{P} \left(\frac{|\gamma|^2}{\text{var}(\gamma)/2} > \frac{\log \eta - \zeta_1}{\varrho_1 \text{var}(\gamma)/2} \middle| \mathcal{H}_1 \right) \\ &= Q_1 \left(\sqrt{\frac{2|\alpha|^2 |\bar{\lambda}_p|^2 \bar{\beta}}{1 + L^{-1} |\alpha|^2 |\bar{\lambda}_d|^2 \bar{\beta}}}, \sqrt{\frac{2(\log \eta - \zeta_1)}{\varrho_1 \text{var}(\gamma)}} \right), \end{aligned} \quad (117)$$

where $Q_1(\cdot)$ denotes the Marcum-Q function of order 1.

By substituting (55) into (117), we have

$$\frac{\log \eta - \zeta_1}{\varrho_1 \text{var}(\gamma)} = L \log \eta - L \zeta_1. \quad (118)$$

By recalling (42), we have

$$-\log \mathbb{P}_{\text{fa}} = L \log \eta - \frac{|\bar{\lambda}_d|^2}{|\bar{\lambda}_p|^2} + L \log \left(1 + \frac{|\bar{\lambda}_d|^2}{L |\bar{\lambda}_p|^2} \right). \quad (119)$$

By invoking (119) into (118), we have $\frac{\log \eta - \zeta_1}{\varrho_1 \text{var}(\gamma)} \approx b_d$.

REFERENCES

- [1] E. Yaacoub and M.-S. Alouini, "A key 6g challenge and opportunity—connecting the base of the pyramid: A survey on rural connectivity," *Proceedings of the IEEE*, vol. 108, no. 4, pp. 533–582, 2020.
- [2] W. Yuan, Y. Cui, J. Wang, F. Liu, G. Sun, T. Xiang, J. Xu, S. Jin, D. Niyato, S. Coleri *et al.*, "From ground to sky: Architectures, applications, and challenges shaping low-altitude wireless networks," *arXiv preprint arXiv:2506.12308*, 2025.
- [3] Y. Jiang, X. Li, G. Zhu, H. Li, J. Deng, K. Han, C. Shen, Q. Shi, and R. Zhang, "Integrated sensing and communication for low altitude economy: Opportunities and challenges," *IEEE Commun. Mag.*, 2025.
- [4] F. Liu, C. Masouros, A. P. Petropulu, H. Griffiths, and L. Hanzo, "Joint radar and communication design: Applications, state-of-the-art, and the road ahead," *IEEE Trans. Commun.*, vol. 68, no. 6, pp. 3834–3862, 2020.
- [5] Y. Cui, F. Liu, X. Jing, and J. Mu, "Integrating sensing and communications for ubiquitous iot: Applications, trends, and challenges," *IEEE network*, vol. 35, no. 5, pp. 158–167, 2021.
- [6] L. Xie, S. Song, Y. C. Eldar, and K. B. Letaief, "Collaborative sensing in perceptive mobile networks: Opportunities and challenges," *IEEE Wireless Commun.*, vol. 30, no. 1, pp. 16–23, 2023.
- [7] 3GPP, "5G; NR; physical channels and modulation," 3rd Generation Partnership Project (3GPP), Technical Specification (TS) 38.211, Jul. 2023, version 17.5.0. [Online]. Available: <http://www.3gpp.org/DynaReport/38211.htm>
- [8] F. Robey, D. Fuhrmann, E. Kelly, and R. Nitzberg, "A cfar adaptive matched filter detector," *IEEE Trans. Aerosp. electro. syst.*, vol. 28, no. 1, pp. 208–216, 1992.
- [9] K. Gerlach, M. Steiner, and F. C. Lin, "Detection of a spatially distributed target in white noise," *IEEE signal processing letters*, vol. 4, no. 7, pp. 198–200, 1997.
- [10] E. Conte, A. De Maio, and G. Ricci, "Glrt-based adaptive detection algorithms for range-spread targets," *IEEE Trans. Signal Process.*, vol. 49, no. 7, pp. 1336–1348, 2002.
- [11] D. R. Fuhrmann, E. J. Kelly, and R. Nitzberg, "A cfar adaptive matched filter detector," *IEEE Trans. Aerosp. Electron. Syst.*, vol. 28, no. 1, pp. 208–216, 1992.
- [12] F. Gini and A. Farina, "Vector subspace detection in compound-gaussian clutter. part i: Survey and new results," *IEEE Trans. Aerosp. Electron. Syst.*, vol. 38, no. 4, pp. 1295–1311, 2003.
- [13] F. Bandiera, A. De Maio, A. S. Greco, and G. Ricci, "Adaptive radar detection of distributed targets in homogeneous and partially homogeneous noise plus subspace interference," *IEEE Trans. Signal Process.*, vol. 55, no. 4, pp. 1223–1237, 2007.
- [14] F. Bandiera, O. Besson, D. Orlando, G. Ricci, and L. L. Scharf, "Glrt-based direction detectors in homogeneous noise and subspace interference," *IEEE Trans. Signal Process.*, vol. 55, no. 6, pp. 2386–2394, 2007.
- [15] D. Ciuonzo, A. De Maio, and D. Orlando, "A unifying framework for adaptive radar detection in homogeneous plus structured interference—part i: On the maximal invariant statistic," *IEEE Trans. Signal Process.*, vol. 64, no. 11, pp. 2894–2906, 2016.
- [16] —, "A unifying framework for adaptive radar detection in homogeneous plus structured interference—part ii: Detectors design," *IEEE Trans. Signal Process.*, vol. 64, no. 11, pp. 2907–2919, 2016.
- [17] G. Ricci, L. L. Scharf *et al.*, "Adaptive radar detection of extended gaussian targets," in *Proc. 12th Annu. Adaptive Sensor Array Process. Workshop*, vol. 1, 2004, pp. 16–18.
- [18] O. Besson, A. Coluccia, E. Chaumette, G. Ricci, and F. Vincent, "Generalized likelihood ratio test for detection of gaussian rank-one signals in gaussian noise with unknown statistics," *IEEE Trans. Signal Process.*, vol. 65, no. 4, pp. 1082–1092, 2016.
- [19] D. Orlando, G. Ricci, and L. L. Scharf, "A unified theory of adaptive subspace detection part i: Detector designs," *IEEE Trans. Signal Process.*, vol. 70, pp. 4925–4938, 2022.
- [20] P. Addabbo, D. Orlando, G. Ricci, and L. L. Scharf, "A unified theory of adaptive subspace detection part ii: Numerical examples," *IEEE Trans. Signal Process.*, vol. 70, pp. 4939–4950, 2022.
- [21] A. Coluccia, G. Ricci, and O. Besson, "Design of robust radar detectors through random perturbation of the target signature," *IEEE Trans. Signal Process.*, vol. 67, no. 19, pp. 5118–5129, 2019.
- [22] J. Liu, K. Wan, X. Yi, R. C. Qiu, and G. Caire, "Blind and topological interference managements for bistatic integrated sensing and communication," *arXiv preprint arXiv:2412.03956*, 2024.
- [23] P. Wang and H. Li, "Target detection with imperfect waveform separation in distributed mimo radar," *IEEE Trans. Signal Process.*, vol. 68, pp. 793–807, 2020.
- [24] L. Xie, P. Wang, S. Song, and K. B. Letaief, "Perceptive mobile network with distributed target monitoring terminals: Leaking communication energy for sensing," *IEEE Trans. Wireless Commun.*, vol. 21, no. 12, pp. 10 193–10 207, 2022.
- [25] Y. Xiong, F. Liu, Y. Cui, W. Yuan, T. X. Han, and G. Caire, "On the fundamental tradeoff of integrated sensing and communications under Gaussian channels," *IEEE Trans. Inf. Theory*, 2023.
- [26] S. Lu, F. Liu, F. Dong, Y. Xiong, J. Xu, Y.-F. Liu, and S. Jin, "Random isac signals deserve dedicated precoding," *IEEE Trans. Signal Process.*, vol. 72, pp. 3453–3469, 2024.
- [27] L. Xie, F. Liu, J. Luo, and S. Song, "Sensing mutual information with random signals in gaussian channels," *IEEE Transactions on Communications*, Early Access, 2025.
- [28] F. Liu, Y. Zhang, Y. Xiong, S. Li, W. Yuan, F. Gao, S. Jin, and G. Caire, "Cp-ofdm achieves the lowest average ranging sidelobe under qam/psk constellations," *IEEE Trans. Inf. Theory*, pp. 1–1, 2025.
- [29] S. Adireddy, L. Tong, and H. Viswanathan, "Optimal placement of training for frequency-selective block-fading channels," *IEEE Trans. Inf. Theory*, vol. 48, no. 8, pp. 2338–2353, 2002.
- [30] C. Xu, X. Yu, F. Liu, and S. Jin, "Exploiting both pilots and data payloads for integrated sensing and communications," 2025. [Online]. Available: <https://arxiv.org/abs/2506.15998>
- [31] P. Wang, J. Fang, H. Duan, and H. Li, "Compressed channel estimation for intelligent reflecting surface-assisted millimeter wave systems," *IEEE Signal Processing Letters*, vol. 27, pp. 905–909, 2020.
- [32] C. Liao, F. Wang, and V. K. Lau, "Optimized design for irs-assisted integrated sensing and communication systems in clutter environments," *IEEE Trans. Commun.*, vol. 71, no. 8, pp. 4721–4734, 2023.
- [33] H. Luo, Y. Wang, D. Luo, J. Zhao, H. Wu, S. Ma, and F. Gao, "Integrated sensing and communications in clutter environment," *IEEE Trans. Wireless Commun.*, vol. 23, no. 9, pp. 10 941–10 956, 2024.
- [34] X. Wang, M. Amin, and X. Cao, "Analysis and design of optimum sparse array configurations for adaptive beamforming," *IEEE Trans. Signal Process.*, vol. 66, no. 2, pp. 340–351, 2017.
- [35] M. R. Akdeniz, Y. Liu, M. K. Samimi, S. Sun, S. Rangan, T. S. Rappaport, and E. Erkip, "Millimeter wave channel modeling and cellular capacity evaluation," *IEEE J. Sel. Areas Commun.*, vol. 32, no. 6, pp. 1164–1179, 2014.